Electronic excitations in thin alkali-metal layers adsorbed on metal surfaces

H. Ishida* and A. Liebsch
Institut für Festkörperforschung, Forschungszentrum Jülich, 5170 Jülich, Germany
(Received 26 July 1991)

The dynamical linear-response properties of realistic Na and K layers adsorbed on a semi-infinite jellium substrate corresponding to the electron density of Al are studied with the aim of elucidating the nature of the adlayer electronic excitations and their variation with coverage. The ground-state properties are described by a first-principles method and the dynamical response in the long-wavelength limit is treated within the time-dependent density-functional approach. At coverages near the work-function minimum, the adsorbate-induced excitations are dominated by intra-atomic excitations between adatom resonant states. Nevertheless, these atomiclike transitions do not lead to any spectral features in the electron-energy-loss function because of the strong hybridization between adatom and substrate states. Instead, as a result of surface screening processes and matrix element effects, a broad loss peak appears near the threshold for emission. This mechanism explains the frequently observed correlation between the coverage dependence of the work function and that of the energy loss induced by the alkali-metal adlayer. As the coverage is increased to one monolayer, the threshold mechanism is replaced by collective excitations consisting of heavily broadened volume plasmons and multipole surface plasmons of the alkali-metal adsorbate. At double-layer coverage, these two modes become very sharp and can clearly be resolved. These collective excitations show only small influence due to the lattice structure of the alkali-metal adlayer.

I. INTRODUCTION

The electronic response of surfaces to weak external fields is one of the most basic topics in surface physics along with the study of structural and electronic properties in the ground state. This field is of interest because it covers important subjects such as surface elementary excitations and the screening of electromagnetic fields, whose knowledge is indispensable for the understanding of observable quantities in a variety of surface spectroscopies.[1,2] Of particular interest is the adsorption of atomic and molecular species on a clean surface. Adsorbates not only modify the response properties of the substrate but also lead to additional excitation modes localized in the adlayer.

The electronic excitations of thin adsorbed alkali metals have been studied for more than 20 years.[3–23] These adsorbates exhibit technologically important properties such as large work-function changes, surface reconstruction, and catalytic promotion.[24,25] In addition, the possibility of varying the average density in the adlayer by changing the adatom coverage Θ has stimulated interest in fundamental problems such as the insulator-metal transition and the collective excitations in quasi-two-dimensional systems. In electron-energy-loss spectroscopy (EELS), excitation modes characteristic of the adlayer have been observed for a wide range of Θ. These excitations show the following general behavior for a number of systems:[26] At very small coverages, the loss features are rather broad; they shift to lower energies with increasing Θ up to a certain coverage around the work-function minimum; for higher Θ, they become rapidly stronger and shift back to higher energies. In the low Θ range, these excitations were traditionally attributed to intra-atomic transitions between the alkali-metal-derived s and p_z states or to transitions involving both substrate and adsorbate states. The rapid growth of loss peaks in the monolayer regime, on the other hand, was often interpreted as due to collective modes in the adlayer. At present, there is no satisfactory understanding of the adlayer excitations. In particular, the actual importance of atomiclike s-p transitions in these systems is not known. Also, the precise nature of the collective modes, their variation with coverage, and their dependency on the lattice structure of the adlayer have yet not been fully investigated.

The main difficulty in surface response theory arises from the nonlocal nature of the response. For the linear response, Feibelman developed a theory in which deviations from the classical local-optics model in the long-wavelength limit are expressed in terms of two functions, $d_\perp(\omega)$ and $d_\parallel(\omega)$.[1,27–29] $d_\perp(\omega)$ is the centroid of the screening density induced by a uniform electric field oriented perpendicular to the surface. Its imaginary part is proportional to the transition rate for creating surface electronic excitations at long wavelength. $d_\parallel(\omega)$ gives the centroid of the z derivative of the current density induced by a uniform electric field parallel to the surface. (We take the z axis as surface normal.) These functions directly determine various quantities observable in surface spectroscopies. In the past, theoretical efforts focused on evaluating the frequency dependence of the d functions mainly for the one-dimensional "jellium" model, where the positive charge of the ionic cores is smeared out into a uniform background charge which drops to zero at the surface.[30] Among the most sophisticated ones are the nonlocal response calculations based on the time-dependent density-functional theory.[31,32] They fully ac-

count for the nonlocal nature of surface response, and treat the ground-state and excitation properties on the same level of approximation. This is necessary in order for surface sum rules for the d functions to hold.[33–35] For the simple metals, these calculations demonstrate that the surface excitation spectra show two features: one near the threshold for emission, i.e., $\omega \approx \Phi$ (work function), and the second near the so-called multipole surface plasmon, $\omega_m \approx 0.8\omega_p$. This latter feature, predicted by Feibelman,[1] is responsible for the local-field enhancement of the surface photoyield[36] and for the enormously enhanced second-harmonic intensity of alkali-metal adsorbates.[20] Analogous response calculations for simple metal surfaces, carried out at finite parallel momentum transfers, recently gave excellent agreement with the measured wave-vector dispersions of the ordinary surface plasmon and of the multipole surface plasmon.[37]

To date, there exist only approximate extensions of these nonlocal response calculations from semi-infinite jellium to more realistic surfaces with three-dimensional lattice structures and to adlayers.[38–42] For alkali-metal adlayers, an approximate way of representing the adlayer is to replace it by a thin jellium slab whose positive background density is proportional to Θ. This "two-step jellium" model was proposed by Lang to study the coverage dependence of the work function.[43] One of us applied this model to study the second-harmonic generation and optical reflectivity problems.[20,21] Very recently, it was used by Liebsch[22] to achieve a systematic understanding of the adlayer collective modes and their variation with coverage. Gaspar *et al.*[23] used the same model and showed how the collective modes of thin alkali-metal adlayers converge on those of clean alkali-metal surfaces as the thickness of the adlayer is increased. The jellium model for the adlayer is mainly appropriate in the full-monolayer range where the orbital overlap among nearby adatoms is sufficiently large. However, it cannot account for the effects of interband and atomiclike transitions which are bound to play the dominant role at low coverages. Several simplified models which approximately account for the atomic nature of the adlayer excitations have been proposed.[14,16,18,19] They are not based, however, on self-consistent descriptions of the electronic density and of the nonlocal response.

To achieve a systematic understanding of the response properties of alkali-metal adlayers, it is clearly necessary to have a theory which can describe atomiclike transitions, interband, and collective excitations on the same footing for a wide range of Θ. As a first step in this direction, we recently studied the linear and nonlinear response of alkali-metal adlayers to a static electric field, using a fully three-dimensional model.[44] In the static limit, the response problem is simplified since it amounts to a ground-state calculation. Thus, it was possible to use a scheme to calculate the ground-state electronic structure of realistic alkali-metal adlayers within the local density-functional theory.[45] The most important result of this work was that those quantities which are related to planar averages, such as the work function and the linear and nonlinear-induced dipole moments, are not very sensitive to the atomic structure within the adlayer, even at coverages as low as $\Theta \approx \frac{1}{4}$. Thus, despite the pronounced atomic corrugation of the actual induced surface densities, these quantities do not deviate significantly from the corresponding results obtained in the jellium model of the adsorbate-substrate system.

In the present work, we go beyond the static limit and determine the dynamical linear-response properties of realistic Na and K adlayers in the long-wavelength limit. Essentially, our scheme combines the self-consistent method of Ishida[46] for the ground-state electronic properties of alkali-metal adlayers with the dynamical-response treatment used by Liebsch[20,21,31] for the jellium versions of adsorbed alkali-metal layers. Thus, the chemisorption bonds and their variation with coverage are accurately described in our scheme. Moreover, the electronic excitations are treated within the time-dependent density-functional approach[47] without any further approximation of the occupied or unoccupied states involved in the transitions. The intra-atomic aspects, the interband contributions, and the collective behavior inherent in these excitations are therefore fully taken into consideration in our calculations. For simplicity, we represent the substrate by the jellium model. The jellium substrate is not particularly meant to model transition-metal substrates with localized d states. However, it may give a sound basis for understanding the essense of those response properties which are rather insensitive to the exact nature of the substrate. Here, we use a bulk density appropriate to Al in order to make contact with a variety of measurements which have been performed for alkali metals adsorbed on Al. The results of these first-principles calculations are compared with dynamical-response calculations carried out for the jellium model of alkali-metal adsorption.

The remarkable and surprising result of the present work is that $\mathrm{Im}d_{\perp}(\omega)$, which is proportional to the EEL intensity at long wavelength, shows no evidence for atomiclike transitions even at the lowest coverage studied here, $\Theta = \frac{1}{4}$, for which the adatom local density of states is already similar to that in the low coverage limit studied by Lang and Williams.[48] In fact, the calculated $\mathrm{Im}d_{\perp}(\omega)$ is nearly identical to that obtained with the two-step jellium model over the entire Θ range. Therefore, we can draw the same conclusion as we did previously in the static limit, namely, that the dynamical dipole moment induced normal to the surface is insensitive to the atomic structure in the adlayer. Of course, at low Θ, the actual induced charge densities are highly corrugated and strongly localized near the adatoms. This means that the screening process is dominated by intra-atomic excitations. However, the occupied adsorbate levels are too strongly broadened via hybridization with the substrate states for any discrete atomiclike peak to appear in $\mathrm{Im}d_{\perp}(\omega)$. Instead, at coverages near the work-function minimum, the spectra show a broad peak at approximately $\omega = \Phi$. The analysis shows that this threshold peak arises from surface screening processes as well as matrix element effects. We are therefore able to understand the common experimental observation, namely, that the ener-

gy of the adlayer excitations correlates with the work function.[26]

As the coverage approaches one monolayer, the threshold feature is replaced by a strong loss peak consisting of adlayer volume and multipole surface-plasmon excitations.[37] However, these modes are so strongly mixed with electron-hole pair excitations that they cannot be resolved. At the double-layer coverage, one can distinguish the adsorbate-vacuum and adsorbate-surface interfaces. As a result, these two collective modes become very sharp and can well be identified in the surface loss function $\mathrm{Im}d_{\perp}(\omega)$. The present calculations demonstrate that the atomic structure within the adsorbate has only small influence on the frequency and width of the collective excitations at monolayer and double-layer coverages.

We also evaluate $d_{\parallel}(\omega)$ using the diagonal approximation which neglects local-field effects. We show that the contribution of $\mathrm{Im}d_{\parallel}(\omega)$ to observable quantities is very small in the energy range relevant for EEL experiments. Nevertheless, $\mathrm{Im}d_{\parallel}(\omega)$, which vanishes identically within the two-step jellium model, diverges as $1/\omega$ in the low-frequency limit. The coefficient of this divergence is directly related to the adlayer-induced change in the resistivity of a thin metallic film which currently attracts much experimental and theoretical attention.[49,50]

The outline of this paper is as follows. In Sec. II, we present the model for the chemisorption of alkali-metal adlayers on a metallic substrate, and describe details of the computational procedure to calculate the linear response of adlayers within the time-dependent density-functional theory. Section III is the main part of the paper. It contains the results of the calculations and a detailed discussion. A summary is given in Sec. IV. Hartree atomic units are used throughout this paper. A preliminary account of the present work has already appeared.[51]

II. THEORY

A. Adlayer model and the Green function

Figure 1 shows the calculational geometry. Our adlayer model is an extension to finite coverages of the work of Lang and Williams,[48] and Hjelmberg, Gunnarsson, and Lundqvist[52] on the single-atom chemisorption on jellium. The electronic structure of alkali-metal adlayers on the semi-infinite jellium is calculated within the local-density approximation in the density-functional theory.[45] In the self-consistent procedure, the embedded region with $b_1 \le z \le b_2$ is treated explicitly, while the effect of the semi-infinite substrate and the vacuum is taken into account via the complex embedding potential invented by Inglesfield.[53] The method is fully three dimensional, and the alkali-ion cores are represented by the norm-conserving pseudopotential.[54] More details of the computational procedure for the ground-state calculation are given in Ref. 46.

With the reciprocal-lattice vectors in the planar direction, $\mathbf{g}$, the Green function

$$G(\mathbf{r},\mathbf{r}',\mathbf{k},\varepsilon)=\langle \mathbf{r}|[\varepsilon+i\delta-H(\mathbf{k},\Theta)]^{-1}|\mathbf{r}'\rangle$$

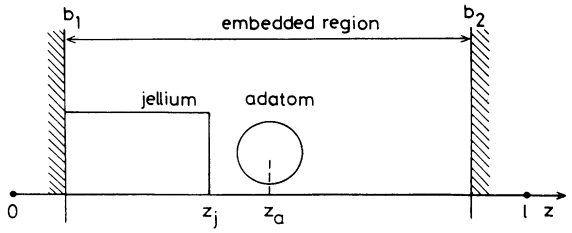

FIG. 1. Calculational geometry for alkali-metal adlayers on semi-infinite jellium.

is expanded as

$$G(\mathbf{r},\mathbf{r}',\mathbf{k},\varepsilon)=\frac{1}{S}\sum_{\mathbf{g},\mathbf{g}'}\exp[i(\mathbf{k}+\mathbf{g})\cdot\mathbf{x}-i(\mathbf{k}+\mathbf{g}')\cdot\mathbf{x}'] \times G(\mathbf{g}z,\mathbf{g}'z',\mathbf{k},\varepsilon)\ , \quad (1)$$

where $\mathbf{x}=(x,y)$, $\mathbf{k}$ is the wave vector in the surface Brillouin zone, ε is the one-electron energy measured from the bottom of the substrate jellium bands, and S denotes the surface area. In the embedding region, $G(\mathbf{g}z,\mathbf{g}'z',\mathbf{k},\varepsilon)$ is expanded using a nonorthogonal sinusoidal basis set (in obvious cases, we omit the indices $\mathbf{k}$ and ε in the Green function):

$$G(\mathbf{g}z,\mathbf{g}'z')=\frac{2}{l}\sum_{n,n'}G(\mathbf{g}n,\mathbf{g}'n')\sin(k_n z)\sin(k_{n'}z') \quad (b_1 \le z,z' \le b_2)\ , \quad (2)$$

where $k_n=n\pi/l$ $(n\ge 1)$. $G(\mathbf{g}n,\mathbf{g}'n')$ is calculated numerically by the inversion of $\varepsilon\bar{S}-\bar{H}$ where $\bar{S}$ and $\bar{H}$ are the overlap and Hamiltonian matrices. Using the Green-function matching technique of Inglesfield,[55] the Green function is then extended into the entire space as follows:

$$G(\mathbf{g}z,\mathbf{g}'z')=\exp[-ik_g(z-b_1)]G(\mathbf{g}b_1,\mathbf{g}'z') \quad (z \le b_1, z' \ge b_1)\ , \quad (3)$$

with

$$k_g=\sqrt{2\varepsilon+i\delta-(\mathbf{k}+\mathbf{g})^2}\ \ (\mathrm{Im}k_g \ge 0)\ , \quad (4)$$

and

$$G(\mathbf{g}z,\mathbf{g}'z')=\frac{\delta_{\mathbf{g}\mathbf{g}'}}{ik_g}\exp(ik_g|z-z'|) + \left[G(\mathbf{g}b_1,\mathbf{g}'b_1)-\frac{\delta_{\mathbf{g}\mathbf{g}'}}{ik_g}\right] \times\exp[-ik_g(z-b_1)-ik_{g'}(z'-b_1)]\ , \quad (z,z' \le b_1)\ . \quad (5)$$

The first term of (5) is the free-electron Green function, whereas the second is the scattering term due to the surface.

B. Linear-response equation

We apply a uniform electric field oriented perpendicular to the surface. Within the time-dependent density-

functional theory,[47] the linearly induced charge density $\delta n(\mathbf{r},\omega)$ satisfies the response equation,

$$\delta n(\mathbf{r},\omega)=\int d\mathbf{r}'\chi_0(\mathbf{r},\mathbf{r}',\omega)[\delta\phi_{\rm cl}(\mathbf{r}',\omega)+\delta V_{\rm xc}(\mathbf{r}',\omega)] . \quad (6)$$

Here $\chi_0(\mathbf{r},\mathbf{r}',\omega)$ is the independent-particle susceptibility, and $\delta\phi_{\rm cl}$ and $\delta V_{\rm xc}$ are the Coulomb and exchange-correlation contributions to the linear potential change:

$$\delta\phi_{\rm cl}(\mathbf{r},\omega)=\phi_{\rm ext}(z,\omega)+\int d\mathbf{r}'\frac{1}{|\mathbf{r}-\mathbf{r}'|}\delta n(\mathbf{r}',\omega) , \quad (7)$$

$$\delta V_{\rm xc}(\mathbf{r},\omega)=\frac{\partial}{\partial n}V_{\rm xc}(n)|_{n_0(\mathbf{r})}\delta n(\mathbf{r},\omega) . \quad (8)$$

In the above, $\phi_{\rm ext}=-2\pi z$ is the external potential, $V_{\rm xc}$ is the local exchange-correlation potential function,[56] and $n_0(\mathbf{r})$ is the ground-state electron density. With the Green function calculated from the self-consistent ground-state potential, χ_0 is expressed as

$$\chi_0(\mathbf{r},\mathbf{r}',\omega)=\frac{-1}{\pi}\int^{E_F}d\varepsilon\int\frac{2d\mathbf{k}}{(2\pi)^2}\mathrm{Im}G(\mathbf{r},\mathbf{r}',\mathbf{k},\varepsilon) \times[G(\mathbf{r},\mathbf{r}',\mathbf{k},\varepsilon+\omega)+G^*(\mathbf{r},\mathbf{r}',\mathbf{k},\varepsilon-\omega)] . \quad (9)$$

The amount of the total induced charge is determined by the bulk dielectric function of the jellium substrate, $\epsilon(\omega)=1-4\pi\bar{n}/\omega^2$, independently of the details of the surface electronic structure. ($\bar{n}>0$ denotes the bulk electron density.) It satisfies

$$\sigma(\omega)=\frac{1}{S}\int d\mathbf{r}\,\delta n(\mathbf{r},\omega)=\frac{\epsilon(\omega)-1}{\epsilon(\omega)+1} . \quad (10)$$

The spectral function $d_\perp(\omega)$ is defined as the centroid of $\delta n(\mathbf{r},\omega)$ measured relative to the substrate jellium edge:

$$d_\perp(\omega)=\frac{1}{S\sigma(\omega)}\int d\mathbf{r}(z-z_j)\delta n(\mathbf{r},\omega) . \quad (11)$$

C. Sum rule for the induced dipole moment

The direct numerical evaluation of $d_\perp(\omega)$ using (11) is not practical because of the Friedel oscillations which $\delta n(\mathbf{r},\omega)$ exhibits in the interior of the metal. For the jellium surface, utilizing the dynamical-force-sum rule,[57] an analytical formula can be derived[31] that relates $d_\perp(\omega)$ to the dipole moment of $\delta n(\mathbf{r},\omega)$ evaluated only in the surface region. We extend this formula to the case where the surface has a three-dimensional adlayer.

Let us consider a thick jellium slab covered by an atomic monolayer on each surface. The adlayers are located at $z=z_a$ and $-z_a$, and the positive background charge fills the space in the range $-z_j\le z\le z_j$. We apply an electric field $E_z=4\pi$ with frequency ω in the z direction. Because the total system is neutral,

$$F_n+F_a+F_j=0 , \quad (12)$$

where F_n, F_a, and F_j denote the forces in the z direction per unit area acting on the electrons, on the ion cores of the adlayers, and on the positive background charge of the jellium slab, respectively. With use of the equation of motion for the electrons, F_n is given as

$$F_n=\frac{1}{S}\sum_i\left\langle\frac{d^2z_i}{dt^2}\right\rangle=\frac{1}{S}\frac{d^2}{dt^2}\int d\mathbf{r}\,zn(\mathbf{r},t)/S , \quad (13)$$

where z_i is the z coordinate of the ith electron, and $n(\mathbf{r},t)$ denotes the total electron density at time t. From (12) and (13), one has for the linearly induced term,

$$\delta F_a+\delta F_j=\omega^2\int_{-\infty}^{\infty}dz\,z\delta\bar{n}(z,\omega) =2\omega^2\int_0^{\infty}(z-z_j)\delta\bar{n}(z,\omega)+2z_j\omega^2\sigma(\omega) , \quad (14)$$

where $\delta\bar{n}(z,\omega)$ denotes the planar average of $\delta n(\mathbf{r},\omega)$.

Next we calculate δF_j and δF_a in an alternative way. δF_j can be evaluated from the induced electric field $d(\delta\phi_{\rm cl})/dz$ as

$$\delta F_j=2(-\bar{n})\int_0^{z_j}dz\,4\pi\left[1-\sigma(\omega)+\int_0^z dz'\delta\bar{n}(z',\omega)\right] =2\omega_p^2\int_0^{z_j}dz(z-z_j)\delta\bar{n}(z,\omega)-2\omega_p^2z_j[1-\sigma(\omega)] , \quad (15)$$

where $\omega_p^2=4\pi\bar{n}$. δF_a is calculated from the linear change in the Hellman-Feynman force acting on an adatom as

$$\delta F_a=\frac{-2}{S_u}\frac{\partial}{\partial z_a}\left[\int d\mathbf{r}[-n_a(\mathbf{x},z-z_a)]\delta\phi_{\rm cl}(\mathbf{r},\omega) +\delta\langle V_{nl}\rangle\right] , \quad (16)$$

where $n_a(\mathbf{x},z-z_a)\ge0$ is the localized positive-charge distribution which represents the local part of the ion-core pseudopotential, $\delta\langle V_{\rm nl}\rangle$ is the linear change in the expectation value of the nonlocal pseudopotential term in the Hamiltonian (per atom), S_u denotes the unit area per adatom, and the prefactor 2 comes from the adlayer in the back surface.

By inserting (15) and (16) into the left-hand side of (14), and noting that the second term on the right-hand side of (14) cancels that of (15) since $\sigma(\omega)=[\epsilon(\omega)-1]/\epsilon(\omega)$ holds for the slab geometry, one has

$$\int_0^{\infty}dz(z-z_j)\delta\bar{n}(z,\omega)=\frac{\epsilon(\omega)-1}{\epsilon(\omega)}\left[\int_{z_j}^{\infty}dz(z-z_j)\delta\bar{n}(z,\omega)-\frac{1}{S_u\omega_p^2}\left[\int d\mathbf{r}\frac{\partial}{\partial z_a}n_a(\mathbf{x},z-z_a)\delta\phi_{\rm cl}(\mathbf{r},\omega)-\frac{\partial}{\partial z_a}\delta\langle V_{\rm nl}\rangle\right]\right] . \quad (17)$$

Since (17) should also hold for the semi-infinite geometry, by dividing (17) by $\sigma(\omega)$, one finally obtains

$$d_\perp(\omega)=\frac{\epsilon(\omega)+1}{\epsilon(\omega)}\left[\int_{z_j}^{\infty}dz\,(z-z_j)\delta\bar{n}(z,\omega)-\frac{1}{S_u\omega_p^2}\left[\int d\mathbf{r}\frac{\partial}{\partial z_a}n_a(\mathbf{x},z-z_a)\delta\phi_{\rm cl}(\mathbf{r},\omega)-\frac{\partial}{\partial z_a}\delta\langle V_{\rm nl}\rangle\right]\right] . \tag{18}$$

The first term in the right-hand side of (18) gives the sum rule for the clean jellium surface.[31] For the jellium adlayer represented by the positive background charge,

$$n_a(z)=\bar{n}_a[\theta(z-z_j)-\theta(z-z_j-d_a)] , \tag{19}$$

the third term in (18) is missing, and one obtains from (18) after some manipulation

$$d_\perp(\omega)=\frac{\epsilon(\omega)+1}{\epsilon(\omega)}\left[\left[1-\frac{\bar{n}_a}{\bar{n}}\right]\int_{z_j}^{\infty}dz\,(z-z_j)\delta\bar{n}(z,\omega)+\frac{\bar{n}_a}{\bar{n}}\int_{z_j+d_a}^{\infty}dz\,(z-z_j-d_a)\delta\bar{n}(z,\omega)\right]+\frac{\bar{n}_a}{\bar{n}}d_a . \tag{20}$$

Let us denote the linear change in the wave function of the one-electron state with energy ε as $\delta\psi_\omega(\mathbf{r},\varepsilon)$. Then, $\delta\langle V_{\rm nl}\rangle$ in (18) is calculated as

$$\begin{aligned}\delta\langle V_{\rm nl}\rangle&=\int^{E_F}d\varepsilon\,d\mathbf{r}\,d\mathbf{r}'\psi^*(\mathbf{r},\varepsilon)V_{\rm nl}(\mathbf{r},\mathbf{r}',z_a)\delta\psi_\omega(\mathbf{r}',\varepsilon)+\int^{E_F}d\varepsilon\,d\mathbf{r}\,d\mathbf{r}'\delta\psi^*_{-\omega}(\mathbf{r}',\varepsilon)V_{\rm nl}(\mathbf{r},\mathbf{r}',z_a)\psi(\mathbf{r}',\varepsilon)\\&=\frac{-1}{\pi}\int^{E_F}d\varepsilon\int d\mathbf{r}\,d\mathbf{r}'d\mathbf{r}''\frac{2d\mathbf{k}}{(2\pi)^2}V_{\rm nl}(\mathbf{r},\mathbf{r}',z_a)\mathrm{Im}G(\mathbf{r},\mathbf{r}'',\mathbf{k},\varepsilon)[G(\mathbf{r}',\mathbf{r}'',\mathbf{k},\varepsilon+\omega)+G^*(\mathbf{r}',\mathbf{r}'',\mathbf{k},\varepsilon-\omega)]\\&\quad\times[\delta\phi_{\rm cl}(\mathbf{r}'',\omega)+\delta V_{\rm xc}(\mathbf{r}'',\omega)] .\end{aligned} \tag{21}$$

It should be noted that if $V_{\rm nl}$ is a local function given as

$$V_{\rm nl}(\mathbf{r},\mathbf{r}',z_a)=V_a(\mathbf{x},z-z_a)\delta(\mathbf{r}-\mathbf{r}') ,$$

Eq. (21) is reduced to an obvious form,

$$\delta\langle V_{\rm nl}\rangle=\int d\mathbf{r}\,V_a(\mathbf{x},z-z_a)\delta n(\mathbf{r},\omega) . \tag{22}$$

D. Computational procedure

Our procedure to solve the response equation (6) is an extension of the method developed in Ref. 31 for jellium surfaces to the three-dimensional case. First, we decompose $\delta\phi_{\rm cl}$ into the two terms as

$$\delta\phi_{\rm cl}(\mathbf{r},\omega)=\phi_b(z,\omega)+\phi_s(\mathbf{r},\omega) , \tag{23}$$

with

$$\phi_b(z,\omega)=-2\pi[1-\sigma(\omega)][z-d_\perp(\omega)] . \tag{24}$$

ϕ_s is taken to vanish in the interior of the metal. In the vacuum, ϕ_s has the asymptotic form

$$\phi_s(\mathbf{r},\omega)=-4\pi\sigma(\omega)[z-d_\perp(\omega)]\quad(z\gg 0) . \tag{25}$$

To account explicitly for the asymptotic behavior of ϕ_s, it is convenient to write

$$\delta n(\mathbf{r},\omega)=\delta n_0(z,\omega)+\delta n_1(\mathbf{r},\omega) , \tag{26}$$

$$\phi_s(\mathbf{r},\omega)=\delta\phi_0(z,\omega)+\delta\phi_1(\mathbf{r},\omega) . \tag{27}$$

In (26), δn_0 is a model charge density having the weight $\sigma(\omega)$ and the dipole moment d_0+id_1, i.e.,

$$\mathrm{Re}\delta n_0(z,\omega)=\sigma(\omega)\frac{\Gamma}{\sqrt{\pi}}\exp[-(z-z_j-d_0)^2\Gamma^2] , \tag{28}$$

$$\begin{aligned}\mathrm{Im}\delta n_0(z,\omega)=&\frac{d_1}{z_1-z_2}\sigma(\omega)\\&\times\{\exp[-(z-z_j-z_1)^2\Gamma^2]\\&-\exp[-(z-z_j-z_2)^2\Gamma^2]\} .\end{aligned} \tag{29}$$

The corresponding Coulomb potential $\delta\phi_0$ is defined as

$$\begin{aligned}\delta\phi_0(z,\omega)&=-4\pi\int_{-\infty}^{z}dz'(z-z')\delta n_0(z',\omega)\\&\to-4\pi\sigma(\omega)(z-d_0-id_1)\quad(z\gg 0) .\end{aligned} \tag{30}$$

The response equation for δn_1 and $\delta\phi_1$ now reads as

$$\delta n_1(\mathbf{r},\omega)=\Delta(\mathbf{r},\omega)+\int d\mathbf{r}'\chi_0(\mathbf{r},\mathbf{r}',\omega)\left[\delta\phi_1(\mathbf{r}',\omega)+\frac{\partial}{\partial n}V_{\rm xc}(n)\Big|_{n_0(\mathbf{r}')}\delta n_1(\mathbf{r}',\omega)\right] , \tag{31}$$

with

$$\Delta(\mathbf{r},\omega)=\xi(\mathbf{r},\omega)-\delta n_0(z,\omega)+\int d\mathbf{r}'\chi_0(\mathbf{r},\mathbf{r}',\omega)\left[\delta\phi_0(\mathbf{r}',\omega)+\frac{\partial}{\partial n}V_{\rm xc}(n)\Big|_{n_0(\mathbf{r}')}\delta n_0(\mathbf{r}',\omega)\right] , \tag{32}$$

where the driving term ξ is defined as

$$\begin{aligned}\xi(\mathbf{r},\omega)&=\int d\mathbf{r}'\chi_0(\mathbf{r},\mathbf{r}',\omega)\phi_b(z',\omega)\\&=-2\pi[1-\sigma(\omega)]\int d\mathbf{r}'z'\chi_0(\mathbf{r},\mathbf{r}',\omega) .\end{aligned} \tag{33}$$

In calculating ξ, one needs to perform the integral over $\mathbf{r}'$ in the entire space. The contribution from the bulk region $z\le b_1$ can be calculated analytically using (3) in the expression of χ_0.

We give a trial input dipole moment $d_{\rm in}=d_0+id_1$. If it is equal to $d_\perp(\omega)$, both δn_1 and $\delta\phi_1$ become localized in the surface. We assume that they are finite only in the embedding region. By inserting (2) into (9), one finds that χ_0 in the embedding region has the form,

$$\chi_0(\mathbf{r},\mathbf{r}',\omega)=\sum_{\mathbf{g},n,\mathbf{g}',n'}\chi_0(\mathbf{g}n,\mathbf{g}'n',\omega)\exp(i\mathbf{g}\cdot\mathbf{x}-i\mathbf{g}'\cdot\mathbf{x}') \times\cos(k_n z)\cos(k_{n'}z') , \tag{34}$$

where $b_1\le z,z'\le b_2$ and $n,n'\ge 0$. In the same way, Δ is expanded as

$$\Delta(\mathbf{r},\omega)=\sum_{\mathbf{g},n}\Delta(\mathbf{g}n,\omega)\exp(i\mathbf{g}\cdot\mathbf{x})\cos(\mathbf{k}_n z)\quad (b_1\le z\le b_2) . \tag{35}$$

These two equations suggest that one should expand δn_1 and $\delta\phi_1$ in the same form,

$$\delta n_1(\mathbf{r},\omega)=\sum_{\mathbf{g}}\exp(i\mathbf{g}\cdot\mathbf{x})\delta n_1(\mathbf{g}z) =\sum_{\mathbf{g}n}\delta n_1(\mathbf{g}n)\exp(i\mathbf{g}\cdot\mathbf{x})\cos(k_n z) , \tag{36}$$

$$\delta\phi_1(\mathbf{r},\omega)=\sum_{\mathbf{g}}\exp(i\mathbf{g}\cdot\mathbf{x})\delta\phi_1(\mathbf{g}z) =\sum_{\mathbf{g}n}\delta\phi_1(\mathbf{g}n)\exp(i\mathbf{g}\cdot\mathbf{x})\cos(k_n z) . \tag{37}$$

By inserting (34)–(37) into (31), one obtains the response equation in the matrix form,

$$\delta n_1(N)=\chi_0(N,N',\omega)C(N',N'')\delta\phi_1(N'') +\chi_0(N,N',\omega)V'_{\rm xc}(N',N'')\delta n_1(N'')+\Delta(N) , \tag{38}$$

where N represents the set of indices $\{\mathbf{g}n\}$, summation is implied for repeated indices, and

$$C(N,N')=\delta_{\mathbf{g}\mathbf{g}'}\int_{b_1}^{b_2}dz\,\cos(k_n z)\cos(k_{n'}z) , \tag{39}$$

$$V'_{\rm xc}(N,N')=\frac{1}{S}\int d\mathbf{x}\int_{b_1}^{b_2}dz\frac{\partial}{\partial n}V_{\rm xc}(n)|_{n_0(\mathbf{r})} \times\exp[-i(\mathbf{g}-\mathbf{g}')\cdot\mathbf{x}]\cos(k_n z)\cos(k_{n'}z) . \tag{40}$$

δn_1 and $\delta\phi_1$ are related by the Poisson equation. Introducing a short-range kernel as in the one-dimensional case, the Poisson equation is written as

$$\delta\phi_1(\mathbf{g}z)=\int_{b_1}^{b_2}dz'\exp(-\kappa_{\mathbf{g}}|z-z'|)\frac{2\pi}{\kappa_{\mathbf{g}}} \times\left[\delta n_1(\mathbf{g}z')+\frac{\kappa^2}{2}\delta\phi_1(\mathbf{g}z')\right] , \tag{41}$$

where

$$\kappa_{\mathbf{g}}=(\kappa^2+|\mathbf{g}|^2)^{1/2} . \tag{42}$$

Equation (41) can be expressed in matrix form as

$$C(N,N')\delta\phi_1(N')=K(N,N')\left[\delta n_1(N')+\frac{\kappa^2}{2}\delta\phi_1(N')\right] , \tag{43}$$

where

$$K(N,N')=\frac{2\pi\delta_{\mathbf{g}\mathbf{g}'}}{\kappa_{\mathbf{g}}}\int_{b_1}^{b_2}dzdz'\cos(\mathbf{k}_n z) \times\exp(-\kappa_{\mathbf{g}}|z-z'|)\cos(k_{n'}z') . \tag{44}$$

Equations (38) and (43) are combined to calculate δn_1 and $\delta\phi_1$, and the output dipole moment $d_{\rm out}$ is calculated with use of the sum rule (18). If we obtain self-consistency, i.e., if $d_{\rm in}=d_{\rm out}$, our assumption that δn_1 and $\delta\phi_1$ are localized near the surface is satisfied. Therefore, $d_\perp(\omega)$ is given by d_0+id_1. The solution should be independent of the parameters, Γ, z_1, z_2, and κ. In practice, we use the higher-dimensional Anderson procedure, reformulated by Blügel[58] in the language of the quasi-Newton method, for the iteration procedure towards self-consistency.

E. Electron-energy-loss intensity

In the dipole scattering approximation, the energy-loss probability in EELS is proportional to the imaginary part of the loss function $g(\mathbf{q}_\parallel,\omega)$. At long wavelength ($\mathbf{q}_\parallel\approx\mathbf{0}$), $g(\mathbf{q}_\parallel,\omega)$ is given[1,27] by

$$g(\mathbf{q}_\parallel,\omega)=\frac{\epsilon(\omega)-1}{\epsilon(\omega)+1}\left[1+2|\mathbf{q}_\parallel|\frac{d_\parallel(\omega)+\epsilon(\omega)d_\perp(\omega)}{\epsilon(\omega)+1}\right] , \tag{45}$$

where $d_\parallel(\omega)$ is the centroid of the z derivative of the current density when a uniform electric field oriented parallel to the wave vector is applied to the system, i.e.,

$$d_\parallel(\omega)=\frac{\int d\mathbf{r}(z-z_j)\frac{\partial}{\partial z}j_\parallel(\mathbf{r},\omega)}{\int d\mathbf{r}\frac{\partial}{\partial z}j_\parallel(\mathbf{r},\omega)} , \tag{46}$$

$$j_\parallel(\mathbf{r},\omega)=\int d\mathbf{r}'\sigma^{\alpha\beta}(\mathbf{r},\mathbf{r}',\omega)E^\beta(\mathbf{r}',\omega) . \tag{47}$$

Here α denotes the direction of $\mathbf{q}_\parallel$ and E^β is the β component of the self-consistent electric field. Within the random-phase approximation, the conductivity tensor $\sigma^{\alpha\beta}$ is expressed as

$$\sigma^{\alpha\beta}(\mathbf{r},\mathbf{r}',\omega)=\sigma_d^{\alpha\beta}(\mathbf{r},\mathbf{r}',\omega)+\sigma_p^{\alpha\beta}(\mathbf{r},\mathbf{r}',\omega) , \tag{48}$$

$$\sigma_d^{\alpha\beta}(\mathbf{r},\mathbf{r}',\omega)=\frac{i}{\omega}n_0(\mathbf{r})\delta_{\alpha\beta}\delta(\mathbf{r}-\mathbf{r}') , \tag{49}$$

$$\sigma_p^{\alpha\beta}(\mathbf{r},\mathbf{r}',\omega)=\frac{i}{\omega}\sum_{i,j}\frac{f_i-f_j}{\varepsilon_i-\varepsilon_j+\omega+i\delta}j_{ij}^\alpha(\mathbf{r})j_{ji}^\beta(\mathbf{r}') , \tag{50}$$

where

$$j_{ij}^\alpha(\mathbf{r})=\frac{1}{2i}\left[\psi_i^*(\mathbf{r})\frac{\partial}{\partial x_\alpha}\psi_j(\mathbf{r})-\left[\frac{\partial}{\partial x_\alpha}\psi_i^*(\mathbf{r})\right]\psi_j(\mathbf{r})\right] . \tag{51}$$

In Eq. (51), ψ_i is the wave function of the one-electron state with energy ε_i, and f_i denotes the Fermi distribution function.

As pointed out by Feibelman,[1] for the quasi-one-dimensional models, the term containing $\sigma_p^{\alpha\beta}$ vanishes after the integration over $\mathbf{r}'$ and $d_\parallel$ becomes a frequency-independent real number. Physically, this means that an electron with momentum $\mathbf{k}$ cannot be scattered to another state with different $\mathbf{k}'$ because of translational invariance in the planar direction. In the present case, where the surface has a three-dimensional adlayer, electrons can be scattered from $\mathbf{k}$ to $\mathbf{k}+\mathbf{g}$. Thus, this term gives rise to a finite complex-current density localized in the surface. Since our main interest is to estimate the order of $\mathrm{Im}d_\parallel(\omega)$, we neglect the local-field corrections (electric fields with nonzero $\mathbf{g}$), and assume $E^\beta(\mathbf{r},\omega)=\delta_{\alpha\beta}E_\parallel$. (As the d-parameter theory is correct only up to the order of $\mathbf{q}_\parallel$, one can ignore the z dependence of $E_\parallel$, which is constant in the range of $1/|\mathbf{q}_\parallel|$.) We then have

$$d_\parallel(\omega)=-\frac{1}{\bar{n}}\int dz\,(z-z_j)\frac{d}{dz}\bar{n}_0(z) - \frac{i\omega}{\bar{n}S}\int d\mathbf{r}\,d\mathbf{r}'\sigma_p^{\alpha\alpha}(\mathbf{r},\mathbf{r}',\omega)\ , \tag{52}$$

where $\bar{n}_0(z)$ is the planar average of $n(\mathbf{r})$, and we integrated by part with respect to z for the second term. Using the Green function (1), Eq. (52) is reexpressed as

$$d_\parallel(\omega)=-\frac{1}{\bar{n}}\int dz\,(z-z_j)\frac{d}{dz}\bar{n}_0(z)-\frac{1}{\bar{n}\pi}\int^{E_F}d\varepsilon\int\frac{2d\mathbf{k}}{(2\pi)^2}\sum_{\mathbf{g},\mathbf{g}'}\int dz\,dz'(\mathbf{k}+\mathbf{g})_\alpha(\mathbf{k}+\mathbf{g}')_\alpha \mathrm{Im}G(\mathbf{g}z,\mathbf{g}'z',\mathbf{k},\varepsilon) \times[G(\mathbf{g}z,\mathbf{g}'z',\mathbf{k},\varepsilon+\omega)+G^*(\mathbf{g}z,\mathbf{g}'z',\mathbf{k},\varepsilon-\omega)]\ , \tag{53}$$

where the integral over z and z' in the bulk region $z,z'\le b_1$ is calculated analytically with (3) and (5). Because of high symmetry, $d_\parallel(\omega)$ does not depend on the direction of $\mathbf{q}_\parallel$ for hexagonal and square adlayers studied in the next section. It will be shown that, in the energy range relevant for EEL experiments on alkali-metal adlayers, $\mathrm{Im}d_\parallel(\omega)$ is actually smaller by several orders of magnitude than $\mathrm{Im}d_\perp(\omega)$. Since $\epsilon(\omega)$ is a real quantity in this energy range, the energy-loss spectrum is essentially proportional to $\mathrm{Im}d_\perp(\omega)$ apart from a kinematical prefactor.[59]

Before closing this section, we discuss the relation between $\mathrm{Im}d_\parallel(\omega)$ and the adlayer-induced change in resistivity of a thin metallic film. We apply a uniform electric field $E_\parallel$ to a metallic film with thickness l_f (100–1000 Å). Introducing the film resistivity ρ, the total energy loss in the film per unit time is given by

$$P=S[l_f\cdot\rho]|J_\parallel|^2=\int d\mathbf{r}\,d\mathbf{r}'\mathrm{Re}\sigma_p^{\alpha\alpha}(\mathbf{r},\mathbf{r}')E_\parallel^2\ , \tag{54}$$

where the macroscopic current in the film, $J_\parallel$, originates from $\sigma_d^{\alpha\alpha}$, i.e.,

$$|J_\parallel|=\frac{\bar{n}}{\omega}E_\parallel\ . \tag{55}$$

From (52), (54), and (55), one finds

$$l_f\rho=-\frac{\omega}{\bar{n}}\mathrm{Im}d_\parallel(\omega)\ . \tag{56}$$

The same result was previously derived by Persson[49] with a phenomenological approach in connection with the lifetime of the frustrated motion of adsorbates parallel to the surface. $l_f\rho$ remains finite in the limit of $\omega\to 0$. As seen from (56), this means that $\mathrm{Im}d_\parallel$ should diverge as $1/\omega$ in the static limit. We note that the local-field correction which we neglected in (52) does not contribute to the divergence of $\mathrm{Im}d_\parallel(\omega)$. Hence, $l_f\rho$ in the static limit is calculated exactly from (52).

III. RESULTS AND DISCUSSION

In the present work, we study Na and K adlayers on semi-infinite jellium with $r_s=2$, which corresponds to the free-electron density of Al. Up to monolayer coverage, the adlayer is assumed to form a hexagonal lattice, and the coverage is varied by changing the lattice constant $a_\parallel$. We define the adlayer with $a_\parallel=7.183$ a.u. as $\Theta_{\mathrm{Na}}=1$ for Na, and the adlayer with $a_\parallel=9.294$ a.u. as $\Theta_{\mathrm{K}}=1$ for K. The distance between the jellium edge and the adlayer, z_a-z_j is chosen as 3.0 and 3.5 a.u. for the Na and K adlayers, respectively. These values correspond to the total-energy minimum obtained by Lang and Williams[42] in the low-coverage limit. Actually, the adlayer exhibits a small outward relaxation with increasing Θ due to the weakening in the adatom-jellium bonding.[60,61] However, since the orbital size of the alkali-metal s and p states are much larger than the amount of this relaxation, it is expected that the response properties of the adlayer change only rather little within this relaxation range.

For the sake of comparison, we perform parallel response calculations for Lang's two-step jellium model.[43] With the above definitions of parameters, the hexagonal adlayers at the full-monolayer coverage have the same electron density as the jellium slab with $r_s=4$ and d_a (slab thickness)$=6$ a.u. for Na, and as the jellium slab with $r_s=5$ and $d_a=7$ a.u. for K, respectively. These jellium slabs were previously used to model the Na and K monolayers in the second-harmonic generation and EEL calculations.[20,22] At low Θ, we fix d_a as above and change the positive-background density of the jellium slab in proportion to Θ.

For Na, we also study the adlayer at the two-monolayer coverage where the second Na layer adsorbs

on the first one. In order to keep the inversion symmetry in the planar direction, the first and second Na layers are assumed to form a square lattice ($a_{\parallel}=6.684$ a.u.) instead of a hexagonal lattice, and Na atoms in the second layer adsorb on the fourfold hollow sites of the first layer. The distance between the jellium edge and the Na layers is chosen as 3 and 9 a.u. for the first and second layers, so that the adlayer has the same electron density as the jellium slab with $r_s=4$ and $d_a=12$ a.u.

We use the following parameter sets: For Na at $\Theta_{\mathrm{Na}}\leq 1$, $b_1=2$, $z_j=10$, $b_2=24$, and $l=26$ a.u.; for Na at $\Theta_{\mathrm{Na}}=2$, $b_1=2$, $z_j=10$, $b_2=30$, and $l=32$ a.u.; for K, $b_1=2$, $z_j=10$, $b_2=26$, and $l=28$ a.u. By virtue of the efficient screening of the substrate (the bulk-plasmon frequency of jellium with $r_s=2$ is 16.65 eV), these parameter sets are found to be sufficient to describe not only the ground-state charge but also the linearly induced charge density as long as ω is smaller than ~ 10 eV. The cutoff energy for the basis functions in expanding the Green function (1) is set to 5 Ry. With this value, the number of basis functions for the largest system is ~ 1000. By making use of symmetry properties, the matrix size of the response equations (38) and (43) can be reduced to ~ 950.

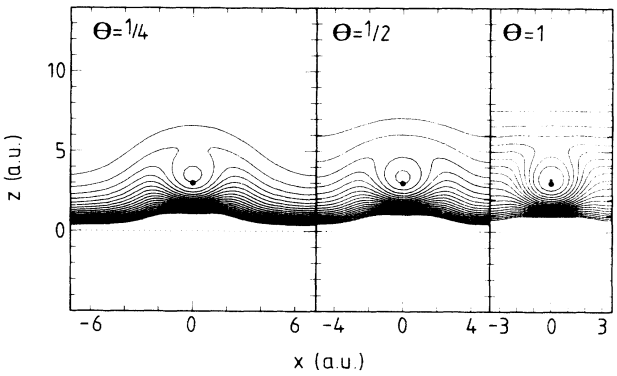

FIG. 2. Contour maps of ground-state charge density $n_0(\mathbf{r})$ for hexagonal Na adlayers on jellium with $r_s=2$ in a plane normal to the surface containing neighboring Na atoms. The contour spacing is 0.0005 a.u. The solid circles and dotted lines indicate the Na nuclei and the jellium edge, respectively. Contours with $n_0(\mathbf{r})\geq 0.01$ are not shown.

A. Ground state

We first discuss briefly the ground-state electronic structure of alkali-metal adlayers. (See Ref. 46 for more details.) Figure 2 shows the contour map of the ground-state charge density for hexagonal Na layers on jellium with $r_s=2$ on a vertical plane containing neighboring adatoms. (The origin of the z axis in this and all subsequent figures is chosen to coincide with the substrate jellium edge.) The charge density is highly corrugated near the adatoms and appears atomiclike at $\Theta_{\mathrm{Na}}=\frac{1}{4}$, whereas the Na valence electrons are almost uniformly distributed in the adlayer at $\Theta_{\mathrm{Na}}=1$. To be accurate, these charge densities are always polarized toward the interface. This causes the electric dipole layer to reduce the work function of the substrate. The calculated work functions Φ are 2.35, 2.55, and 3.20 for $\Theta_{\mathrm{Na}}=\frac{1}{4}$, $\frac{1}{2}$, and 1, respectively. For the present system, the minimum of the work function occurs at $\Theta_{\mathrm{Na}}\approx 0.35$.

The Θ dependence of the adatom electronic structure is more clearly seen in the adatom local density of states, $\rho_a(\varepsilon,\Theta)$, and the dipole density of states, $\mu_a(\varepsilon,\Theta)$, which are defined as

$$\rho_a(\varepsilon,\Theta)=\int_R d\mathbf{r}\int d\mathbf{k}\frac{2}{(2\pi)^2}\mathrm{Im}[G(\mathbf{r},\mathbf{r},\mathbf{k},\varepsilon)|_{\Theta}-G(\mathbf{r},\mathbf{r},\mathbf{k},\varepsilon)|_{\Theta=0}]\ , \tag{57}$$

$$\mu_a(\varepsilon,\Theta)=\int_R d\mathbf{r}(z-z_a)\int d\mathbf{k}\frac{2}{(2\pi)^2}\mathrm{Im}[G(\mathbf{r},\mathbf{r},\mathbf{k},\varepsilon)|_{\Theta}-G(\mathbf{r},\mathbf{r},\mathbf{k},\varepsilon)|_{\Theta=0}]\ , \tag{58}$$

where the integral over $\mathbf{r}$ is performed in a small adatom sphere with radius R. One-electron states with positive (negative) μ_a are polarized toward the interface (vacuum) side of the adlayer and, therefore, may be regarded as bonding (antibonding) states with respect to the adatom-substrate bonding. The calculated ρ_a and μ_a for Na adlayers are shown in Fig. 3(a). At $\Theta_{\mathrm{Na}}=\frac{1}{4}$, ρ_a has two atomiclike resonances above E_F. It is already similar to ρ_a given by Lang and Williams[48] in the low Θ limit. Thus, the direct Na-Na interaction is fairly small at this coverage. The lower peak corresponds to the hybridized state of Na $3s$ and $3p_z$, and the higher one is Na $3p_{\parallel}$.

It is important that, owing to the strong interaction between the substrate states and adatom orbital with σ symmetry, Na $3s$ and $3p_z$, which are not good quantum numbers for the adatom, do not form separate resonances. Therefore, for the present system, there is no reason to expect that a loss peak appears at the energy close to the energy separation between the $3s$ and $3p_z$ levels of a free Na atom.

While ρ_a is smooth and has no particular structure at E_F, μ_a changes its sign very rapidly near E_F. The hybridized $3s$-$3p_z$ resonance is seen to be an antibonding state whose wave function is strongly polarized towards the vacuum. It is thus expected that the excitations from the occupied bonding states to the antibonding resonance have large dipole matrix elements leading to an induced charge localized on the vacuum side of the adatoms. With increasing Θ, the atomic peaks in ρ_a are smeared out because of the formation of wide adlayer bands. The broadening of the peaks, however, does not imply the disappearance of resonances. They are still sharp if ρ_a is decomposed in $\mathbf{k}$ space. The band width of the lowest hybridized $3s$-$3p_z$ state along the $\bar{\Gamma}$-$\bar{K}$ line in the surface

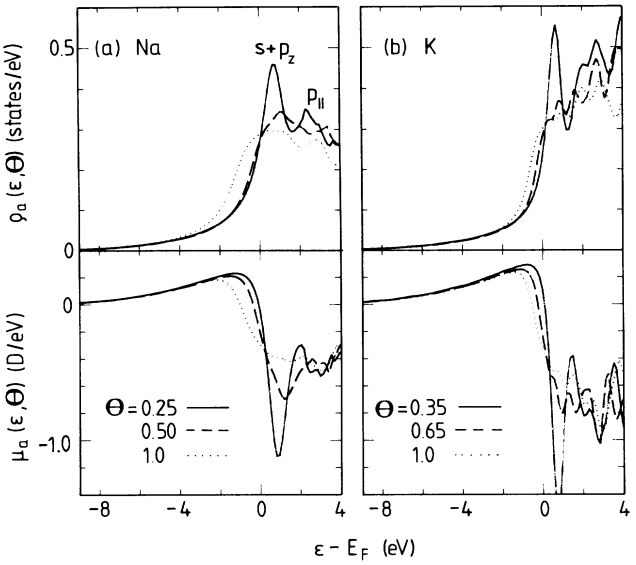

FIG. 3. Adatom density of states $\rho_a(\varepsilon,\Theta)$ and dipole density of states $\mu_a(\varepsilon,\Theta)$ for (a) Na and (b) K adlayers on jellium with $r_s=2$.

Brillouin zone is 0.4, 1.6, and 3.7 eV for $\Theta_{Na}=\frac{1}{4}$, $\frac{1}{2}$, and 1, respectively. The area of the occupied part of ρ_a is almost constant up to $\sim\Theta_{Na}=0.7$, while the large overlap of the valence charge among nearby adatoms leads to its appreciable increase at $\Theta_{Na}=1$. In Fig. 3(b) we show ρ_a and μ_a for K adlayers. Their qualitative features are similar to those in the densities of states for Na, except that ρ_a and μ_a for K above E_F is much more complicated due to the low-lying d states.

B. Induced density and potential

Figures 4(a)–4(c) show contour maps of the real part of the normalized induced charge density $\delta n(\mathbf{r},\omega)/\sigma(\omega)$ for Na on jellium with $r_s=2$ as a function of ω for three adlayers in the same plane as in Fig. 2. Note that $\mathrm{Re}\delta n/\sigma$ is normalized to unity when integrated over a unit cell independently of Θ and ω. The solid, dashed, and dot-dashed contours correspond to positive, negative, and zero values, respectively, and the contour spacing is 0.08 a.u. The contour maps at the lowest frequency ($\omega=1$ eV) are very similar to those of the linearly induced charge in our previous work calculated in the static limit ($\omega=0$) for Na on jellium with $r_s=3$,[44] except that the Friedel oscillations which δn exhibits in the substrate have a shorter wavelength because of the higher jellium density used in the present work.

First we discuss the Θ dependence of $\mathrm{Re}\delta n$. At $\Theta_{Na}=\frac{1}{4}$ and low ω, $\mathrm{Re}\delta n$ has a localized peak with a large amplitude on the vacuum side of the Na atoms. The peak height is ~ 4 times larger than the planar average of the induced density at the same z coordinate. As discussed in the static limit,[44] the kidney-shaped-induced density can be understood as resulting from excitations to the hybridized s-p_z resonance since its wave function is strongly polarized toward the vacuum. Therefore, at low ω, the screening of the external field is dominated by intra-atomic excitations between adatom resonances. With increasing Θ, the induced density exhibits a continuous transition to a more uniform charge distribution in the planar direction.

Next, we discuss the ω dependence of $\mathrm{Re}\delta n$. At low ω, $\mathrm{Re}\delta n$ is located mostly on the vacuum side of the Na plane irrespective of Θ, reflecting the efficient screening due to Na valence electrons. The applied field cannot penetrate into the adlayer in this ω range. Up to a certain frequency which strongly depends on Θ, the centroid of $\delta n/\sigma$ shifts slightly toward the vacuum. Then it starts to move inward and crosses the plane of Na nuclei. When the centroid of $\mathrm{Re}\delta n$ moves across the Na plane, the density becomes strongly distorted near the Na nuclei in such a way that δn is repelled from the Na cores (e.g., see $\delta n/\sigma$ at $\omega=6$ eV at $\Theta_{Na}=1$). This behavior is caused by the repulsive Na pseudopotential. For higher ω, the adlayer becomes essentially transparent to the applied field. $\mathrm{Re}\delta n$ becomes negative on the vacuum side of the adlayer, and the screening is caused by the fairly uniform induced charge built up at the substrate-adsorbate interface.

In Figs. 4(d)–4(f) we show contour maps of $\mathrm{Im}\delta n(\mathbf{r},\omega)/\sigma(\omega)$. Since $\sigma(\omega)$ is a real quantity, $\mathrm{Im}\delta n$ vanishes when integrated over a unit cell. $\mathrm{Im}\delta n$ disappears also in the static limit as χ_0 is a real function when $\omega=0$ [see (9)]. $\mathrm{Im}d_\perp(\omega)$ is given by the dipole potential barrier caused by these charge distributions. Again, one clearly sees in these contour maps the continuous transition from atomiclike response at low Θ to laterally more uniform response at higher Θ. In contrast to $\mathrm{Re}\delta n/\sigma$, the shape of these contour maps does not show a strong ω dependence, except that the induced charge becomes slightly negative on the vacuum region at the highest ω. On the other hand, the amplitude of $\mathrm{Im}\delta n/\sigma$ depends greatly on ω. It reaches its maximum in the ω range where the centroid of $\mathrm{Re}d_\perp(\omega)$ crosses the Na plane. This resonant behavior is expected, since $\mathrm{Re}d_\perp(\omega)$ and $\mathrm{Im}d_\perp(\omega)$ are related via a Kramers-Kronig relation.[35] The origin of this resonant peak will be discussed in detail below.

The solid curves in Fig. 5 show the planar average of the real part of the induced charge density, $\delta\bar{n}(z,\omega)/\sigma(\omega)$ for Na adlayers as a function of ω. They are compared with the corresponding induced densities calculated using the two-step jellium model, which are one-dimensional from the beginning (dashed curves). Except for $\Theta_{Na}=\frac{1}{4}$ where the atomic character of the excitations is dominant, the agreement with the solid curves is surprisingly good, especially at low frequencies. This is so despite the fact that the actual induced charge at $\Theta_{Na}=\frac{1}{2}$ is appreciably corrugated as shown in Fig. 4. Therefore, the two-step jellium model can describe planar averages of linear response properties of real alkali-metal adlayers quite well for coverages higher than the work-function minimum. This was also the case in the static limit.[44]

In the upper panels of Fig. 6, we show contour maps of the real part of the normalized Hartree potential, $\delta\phi_{cl}(\mathbf{r},\omega)/\sigma(\omega)$ at $\Theta_{Na}=\frac{1}{4}$ for several frequencies. It can

clearly be seen how the external electric field is screened out by the induced densities. In the vacuum region, the potential decreases linearly with the slope, $-2\pi(1+\sigma(\omega))/\sigma(\omega)$. With increasing ω, the electric field penetrates more into the interior of the adlayer since the screening becomes less efficient. Because of the long-range nature of the Coulomb potential, the three-dimensional corrugations of $\delta\phi_{\rm cl}$ are much less pronounced than those in the corresponding contour maps of δn in Fig. 4.

The lower panels of Fig. 6 show the corresponding contour maps of the real part of the total self-consistent potential,

$$\phi_{\rm SCF}(\mathbf{r},\omega)=\delta\phi_{\rm cl}(\mathbf{r},\omega)+\delta V_{\rm xc}(\mathbf{r},\omega)\ , \tag{59}$$

divided by $\sigma(\omega)$. Here, the one-dimensional nature of the potential is much more enhanced because of significant cancellations of $\delta\phi_{\rm cl}$ and $\delta V_{\rm xc}$. As a result, the atomic-like nature of the contours seen in $\delta\phi_{\rm cl}$ on the vacuum side of the Na plane at low ω is entirely absent in the cor-

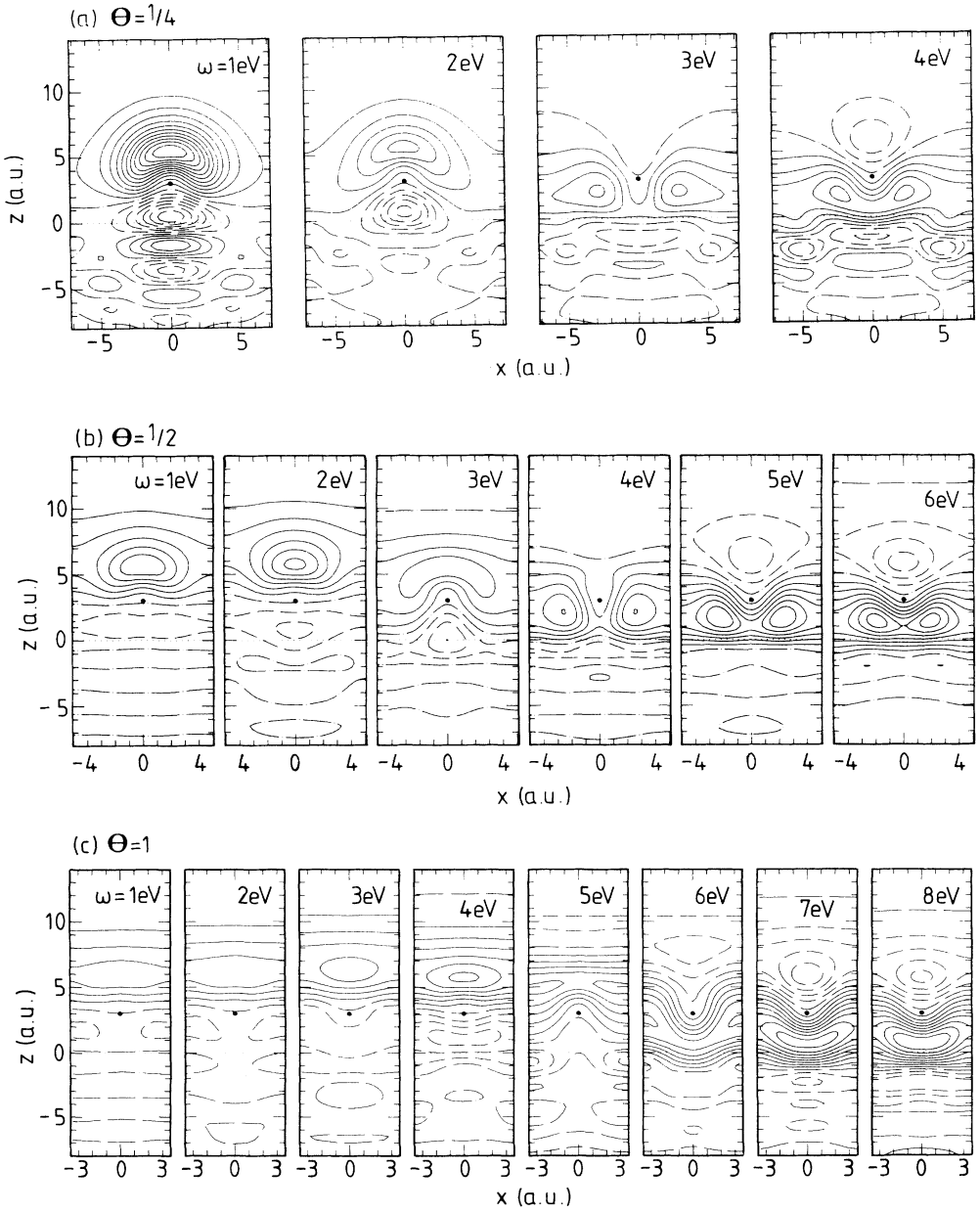

FIG. 4. (a)–(c) Contour maps of the real part of induced density $\delta n(\mathbf{r},\omega)$ for hexagonal Na layers on jellium with $r_s=2$ on the same cut plane as in Fig. 2 as functions of Θ and ω. The solid, dashed, and dot-dashed contours correspond to positive, negative, and zero values. The contour spacing is 0.08 a.u. (d)–(f) Corresponding contour maps of the imaginary part of $\delta n(\mathbf{r},\omega)$.

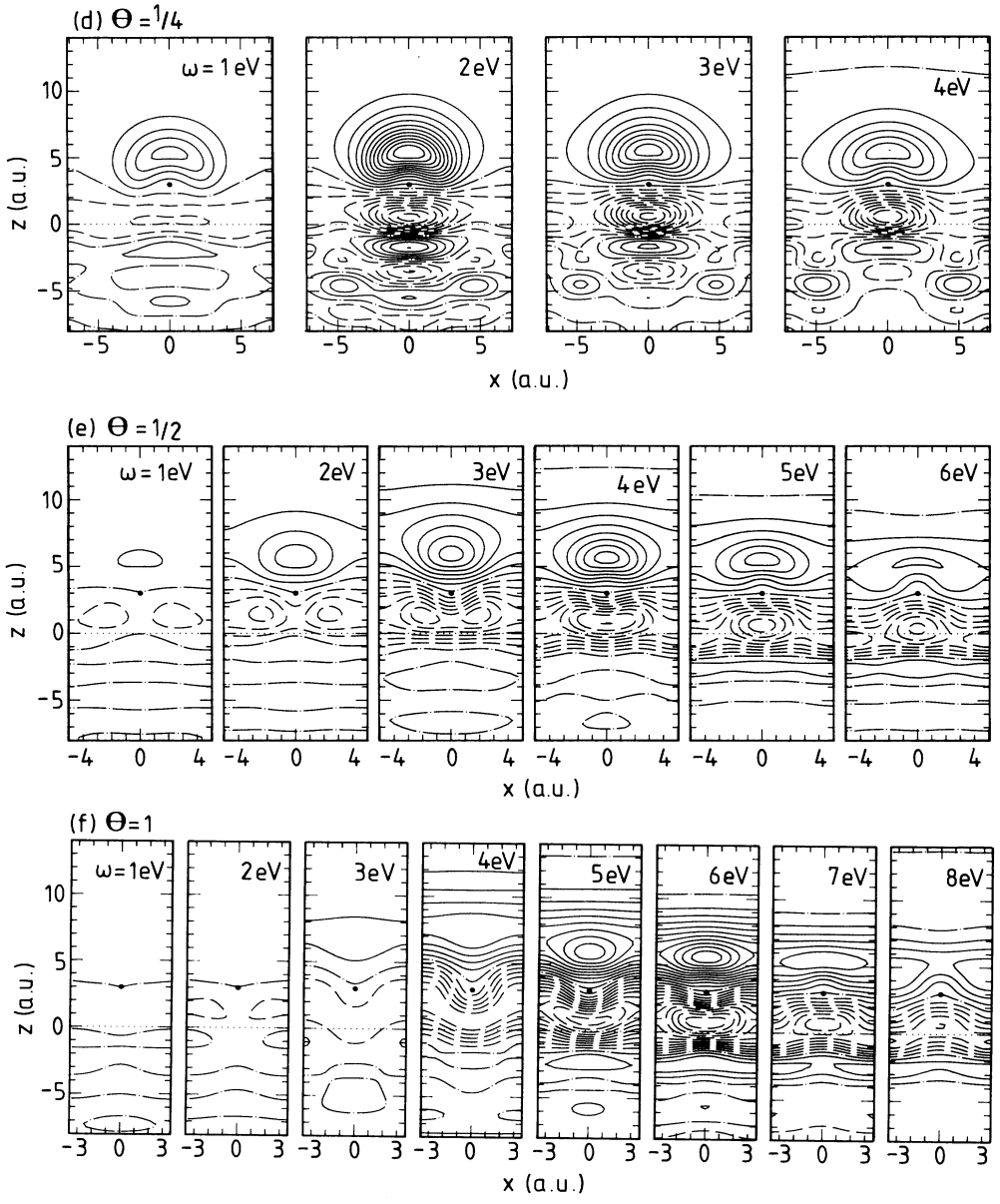

FIG. 4. (*Continued*).

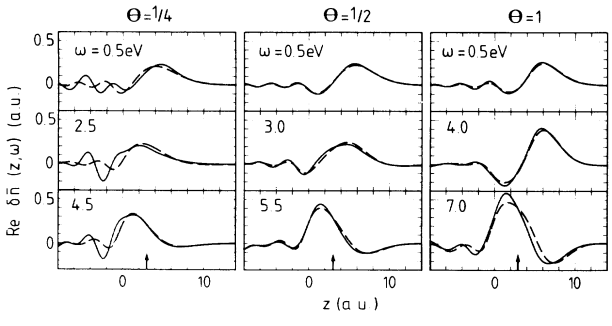

FIG. 5. Planar average of induced density, $\delta\bar{n}(z,\omega)$ for Na adlayers (solid curves). The dashed curves are induced densities calculated with the corresponding one-dimensional jellium adlayers. The arrows denote the positions of the Na nuclei.

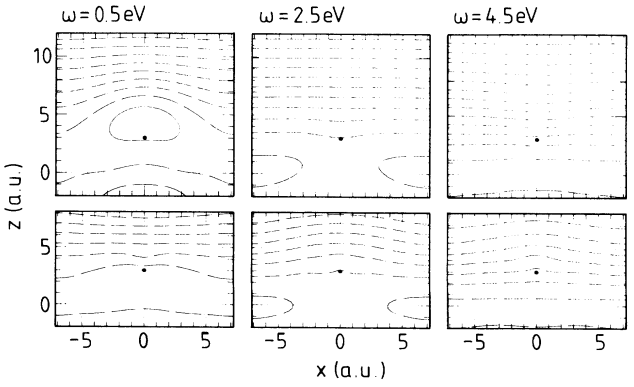

FIG. 6. Contour maps of the real part of induced Coulomb potential $\delta\phi_{\rm cl}(\mathbf{r},\omega)$ for Na at $\Theta_{\rm NA}=\frac{1}{4}$ (upper panels). Corresponding contour maps of real part of self-consistent potential $\phi_{\rm SCF}(\mathbf{r},\omega)$ (lower panels). The contour spacing is 10 a.u.

responding contour map of $\mathrm{Re}\phi_{\mathrm{SCF}}/\sigma$. The one dimensionality of the potential is further enhanced at higher Θ. Therefore, the essential features of ϕ_{SCF} can be understood from its planar average shown in Fig. 7. In contrast to the induced densities shown in Fig. 5, these potential curves show no Friedel oscillations in the interior of the metal. As compared with $\delta\phi_{\mathrm{cl}}$, the positions where the potential starts to decrease are shifted by 2–3 a.u. toward the metal side due to negative contribution of δV_{xc}. Nevertheless, as a result of screening processes, $\phi_{\mathrm{SCF}}(\mathbf{r},\omega)$ at low frequencies nearly vanishes on the interface side of the Na nuclei, where one-electron wave functions of the occupied states have larger weight because of the Na-jellium bonding. At higher Θ, this potential penetrates the adlayer even less, i.e., it is finite only in the outer regions of the adlayer-vacuum interface. As will be discussed below, this behavior has important consequences for the ω dependence of the adlayer excitations. With increasing ω, these potential curves shift slightly outward up to a certain frequency and then shift rapidly backward, corresponding to the resonant behavior of $\mathrm{Re}\delta n(\mathbf{r},\omega)$ discussed above. At the same time, since the external field is overscreened in the present ω range $[\sigma(\omega)\geq 1]$, the potential shows a positive slope inside the metal.

C. Spectral functions: $d_\perp(\omega)$ and $d_\parallel(\omega)$

The real and imaginary parts of the centroid $d_\perp(\omega)$ of the induced density for Na adlayers are shown in Fig. 8 from $\Theta_{\mathrm{Na}}=\frac{1}{4}$ to 2. They are compared with $d_\perp(\omega)$ calculated for the corresponding jellium adlayers. The area of $\mathrm{Im}d_\perp(\omega)$ in the energy range characteristic of adsorbate excitations increases monotonically with increasing number of adatoms. For jellium surfaces, Persson and Zaremba[35] derived an f-sum rule for $\mathrm{Im}d_\perp(\omega)$. Their formula

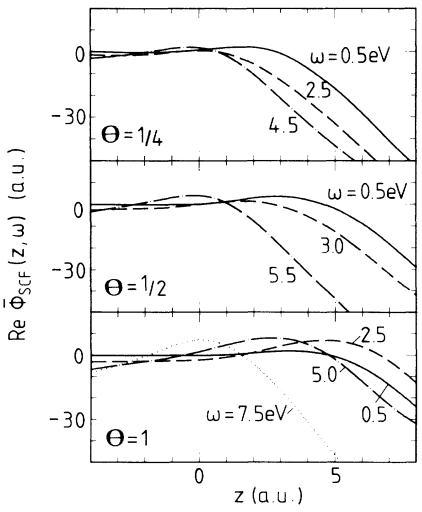

FIG. 7. Planar average of self-consistent potential, $\bar{\phi}_{\mathrm{SCF}}(z,\omega)$ for Na adlayers on jellium with $r_s=2$ as functions of Θ and ω.

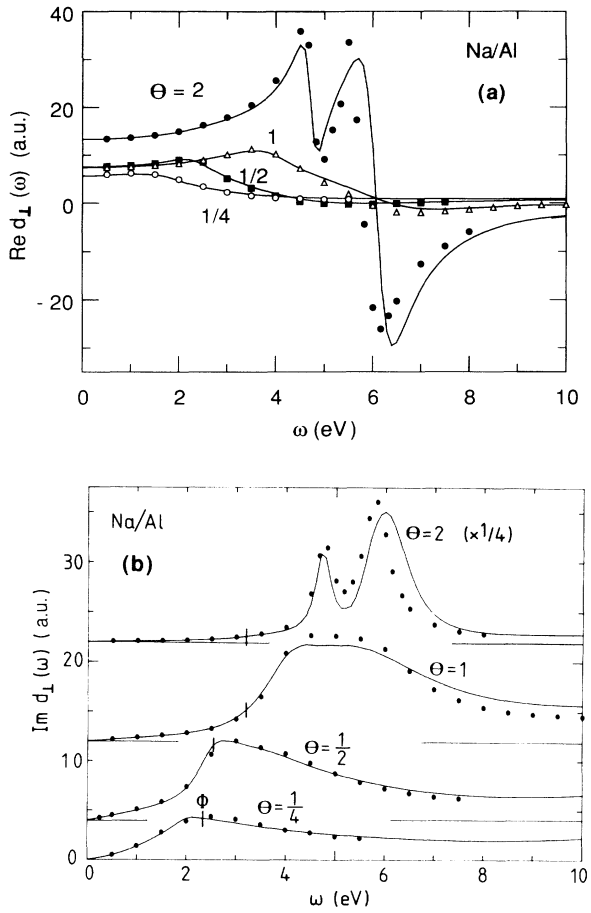

FIG. 8. (a) Real and (b) imaginary parts of spectral function $d_\perp(\omega)$ for Na-covered jellium surfaces (symbols). The solid lines show $d_\perp(\omega)$ for the corresponding one-dimensional model calculations. The vertical dashes in (b) denote the work function.

can be extended to the case of the two-step jellium model as,

$$\frac{2}{\pi}\int_0^\infty d\omega\,\omega\,\mathrm{Im}d_\perp(\omega)=4\pi\bar{n}\lambda\ , \tag{60}$$

where λ is expressed in terms of the ground-state density $n_0(z)$ as

$$\lambda=\left[1-\frac{\bar{n}_a}{\bar{n}}\right]\int_{zj}^{z_j+d_a}dz\,n_0(z)+\int_{z_j+d_a}^{\infty}dz\,n_0(z)\ . \tag{61}$$

If the adlayer thickness d_a is large enough, the second term of (61) does not depend on d_a and gives the same value as λ for clean alkali-metal surfaces. Then λ increases linearly with the slope $(1-\bar{n}_a/\bar{n})\bar{n}_a$ as a function of d_a. This slope takes a maximum value of $0.25\bar{n}_a$ when $\bar{n}_a=0.5\bar{n}$.

The comparison of $d_\perp(\omega)$ with the results of the two-step jellium model demonstrates that the spectral function $\mathrm{Im}d_\perp(\omega)$ shows no evidence of atomiclike excitations, even at low Θ. The atomic structure of the adlayer is seen to cause only a slight narrowing of the spectral features. This narrowing signifies that the wave functions of Na valence states are actually more tightly bound in

the adlayer region than described by the jellium model (especially the unoccupied states), so that the jellium model overestimates the damping of adlayer excitations due to coupling to electron-hole pair excitations at the substrate-adsorbate interface.

First, we discuss the collective excitations in the adlayer. For an adsorbate double layer ($\Theta_{Na}=2$), the adlayer-substrate and adlayer-vacuum interfaces are well separated. Thus two adlayer-induced collective modes are found: one at the Na volume plasma frequency, $\omega_p=\omega_p(\text{ads})$, which is the analog of the $\mathbf{q}_\parallel=0$ mode in the local-optics model,[11] and the other at $\omega_m(\text{ads})\approx 0.8\omega_p(\text{ads})$ due to the multipole surface plasmon at the adlayer-vacuum interface. Note that the energy of the lower mode, in the long wavelength limit, does not approach the surface plasma frequency, $\omega_s=\omega_p(\text{ads})/\sqrt{2}$, even for a thicker adlayer. The ordinary (monopole) surface plasmon arising from the classical boundary condition $\varepsilon(\omega)+1=0$ appears at $\omega_p(\text{sub})/\sqrt{2}$ (11.8 eV in the present system). On the other hand, it was recently shown[22] within the two-step jellium model that the two adlayer-induced volume and multipole surface-plasmon modes exhibit a negative energy dispersion at small $\mathbf{q}_\parallel$ and that their frequencies converge to those of the multipole and monopole surface-plasmon modes of the semi-infinite alkali-metal surfaces at $\mathbf{q}_\parallel\approx 1/d_a$. For thicker d_a, we expect that more Na bulk plasmons with different wavelengths in the z direction may contribute to $\text{Im}d_\perp(\omega)$, since λ increases linearly with d_a.

At $\Theta_{Na}=1$, the planar average of the ground-state density does not show a plateau in the adlayer region. As a result, the adlayer volume and multipole surface-plasmon modes become heavily broadened due to coupling to electron-hole pairs. Therefore, only one asymmetric spectral peak remains. Finally, at coverages near the work-function minimum, the average density of the adlayers is much smaller and the spectral weight associated with collective modes has nearly vanished. Instead, the excitation spectra are dominated by a broad peak near the threshold for emission, i.e., near $\omega\approx\Phi$.

While the collective behavior of the excitations at higher Θ is not surprising, the absence of any atomiclike peak in $\text{Im}d_\perp(\omega)$ at $\Theta_{Na}=\frac{1}{4}$ is indeed an unexpected result of the three-dimensional response calculation. Since $\rho_a(\varepsilon,\Theta)$ at $\Theta_{Na}=\frac{1}{4}$ is already very similar to that in the single adatom limit, we do not assume that atomiclike structures become more prominent in the surface loss function at even lower Θ. Of course, as was shown above, the screening processes are dominated by intraatomic excitations from the occupied bonding states to the hybridized Na $3s$-$3p_z$ resonance at low Θ. The peak in the Na local density of states, $\rho_a(\varepsilon,\Theta)$, due to this resonance which is located ~ 1 eV above E_F, is rather sharp. However, since the occupied part of the Na-state density exhibits only a broad taillike structure due to the strong adatom-substrate chemical interaction, these atomic transitions do not lead to observable spectral features in the response function $\text{Im}d_\perp(\omega)$.

Therefore, at least for alkali-metal adsorption on Al, the traditional interpretation[8,9] that the observed loss peak in EELS should be assigned to an excitation between alkali-metal s and p_z states or to an excitation from E_F to the unoccupied resonance, must be regarded as incorrect. We expect this conclusion to hold also at finite wave vectors ($|\mathbf{q}_\parallel|\leq 0.2$ Å^{-1}) since the field oscillations in the planar direction are much longer than the atomic corrugation. In the case of transition-metal substrates such as W or Ni, atomiclike features in the loss function may become more prominent because of weaker adatom-substrate hybridization or because of the formation of quasi-discrete adsorbate surface states. Also, intraatomic excitations may be somewhat more important for Cs adlayers because of the larger separation from the substrate. Further study is necessary in this direction.

Having demonstrated the absence of atomiclike peaks in $\text{Im}d_\perp(\omega)$ at low Θ, we need to answer the question of why this spectral function shows a peak at $\omega\approx\Phi$. To analyze the origin of this behavior, it is useful to express $\text{Im}d_\perp(\omega)$ using the golden-rule formula,[62]

$$\text{Im}d_\perp(\omega)=\frac{1}{2\pi\sigma(\omega)[\sigma(\omega)+1]}\times\int d\mathbf{r}\,d\mathbf{r}'\phi^*_{\text{SCF}}(\mathbf{r},\omega)\text{Im}\chi_0(\mathbf{r},\mathbf{r}',\omega)\phi_{\text{SCF}}(\mathbf{r}',\omega)\ . \tag{62}$$

This may be written as a sum over transition-matrix elements of the form

$$v(\varepsilon,\omega,\mathbf{k})=\sum_{i,j}\left|\int d\mathbf{r}\,\psi^*_{\varepsilon,\mathbf{k},i}(\mathbf{r})\phi_{\text{SCF}}(\mathbf{r},\omega)\psi_{\varepsilon+\omega,\mathbf{k},j}(\mathbf{r})\right|^2, \tag{63}$$

with initial states in the range $E_F-\omega\leq\varepsilon\leq E_F$. Here $\psi_{\varepsilon,\mathbf{k},i}(\mathbf{r})$ denotes the one-electron wave function with energy ε at $\mathbf{k}$, and the indices i and j distinguish the degenerate states. If the effective potential ϕ_{SCF} is replaced by the unscreened external potential, the excitation spectra at all coverages are smooth functions of ω without any features at Φ, $\omega_m(\text{ads})$, and $\omega_p(\text{ads})$. Thus the threshold excitation found at low Θ is not a density-of-states effect related to the shape of the ground-state surface-barrier potential at the vacuum level. Instead, this peak is intimately connected with the fact that ϕ_{SCF} has appreciable weight only on the vacuum side of the adlayer (see Fig. 7). As a result of electronic surface screening, the transition-matrix elements (63) probe effectively only the outer regions of the occupied and unoccupied adsorbate wave functions.

This effect is shown in more detail in Fig. 9. In panel (a), $\text{Im}d_\perp(\omega)$ at $\Theta_{Na}=\frac{1}{4}$ is plotted for various cutoffs z_0 (measured from the jellium edge), i.e., the contribution to the matrix elements from the regions $z\leq z_0$ is neglected. Also, $\phi_{\text{SCF}}(\mathbf{r},\omega)$ is replaced by its planar average. The spectral feature near $\omega\approx\Phi$ remains discernible even if z_0 is located on the vacuum side of the Na nuclei, i.e., far from the center of the bonding region of the adsorbate-substate states. In Fig. 9(b), we show $v(\varepsilon=E_F,\omega,\mathbf{k}=\mathbf{0})$ at $\Theta_{Na}=\frac{1}{4}$ which gives the most important contribution to $\text{Im}d_\perp(\omega)$. If the threshold for emission is approached from below, the amplitude of the unoccupied state in the outer region of the adlayer-vacuum interface grows so

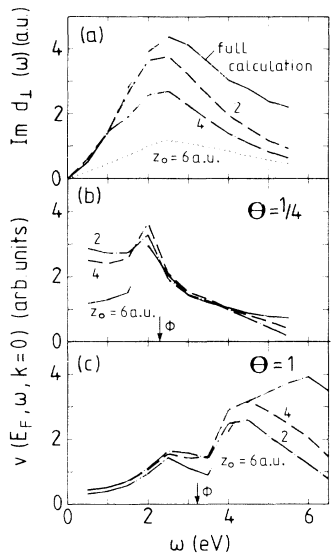

FIG. 9. (a) $\mathrm{Im}d_\perp(\omega)$ for Na on jellium ($r_s=2$) at $\Theta_{\mathrm{Na}}=\frac{1}{4}$ for various cutoffs z_0 (see text). (b) Matrix element $v(E_F,\omega,\mathbf{k}=0)$ for Na at $\Theta_{\mathrm{Na}}=\frac{1}{4}$. (c) $v(E_F,\omega,\mathbf{k}=0)$ for Na at $\Theta_{\mathrm{Na}}=1$.

that the matrix element increases. Above threshold, the continuum states oscillate more rapidly and the matrix element eventually begins to decrease. Thus, the matrix elements reach their maxima when $\omega\approx\Phi$. For the sake of comparison, we show in Fig. 9(c) $v(E_F,\omega,\mathbf{k}=0)$ at $\Theta_{\mathrm{Na}}=1$. The threshold enhancement of the matrix element is clearly seen also in this case, although it appears ~ 0.5 eV below Φ. Upon integration over initial states, this feature is suppressed. Instead, a peak at higher ω corresponding to the plasmon modes arises from the ω dependence of $\phi_{\mathrm{SCF}}(\mathbf{r},\omega)$. Thus, the two peaks in this figure have quite different origins.

To make the above argument more quantitative, we consider a one-dimensional model with the ground-state potential, $V(z)=-V\theta(-z)$. As ϕ_{SCF}, we adopt a simple screened form, $\phi_{\mathrm{SCF}}=(z-z_0)\theta(z-z_0)$, with $z_0>0$. The initial-state energy is chosen as $\varepsilon_i=-k_i^2/2$ (measured from the vacuum level). In case the final state is also a bound state with $\varepsilon_f=-k_f^2/2$, we have

$$v(\varepsilon_i,\omega=\varepsilon_f-\varepsilon_i)=\frac{2\sqrt{2V-k_f^2}\exp[-2(k_i+k_f)z_0]}{V(k_i+k_f)^4}\ . \tag{64}$$

For $\varepsilon_f=k_f^2/2>0$, there are two orthogonal final states which contribute to the matrix elements. After some calculations, we obtain

$$v(\varepsilon_i,\omega=\varepsilon_f-\varepsilon_i)=\frac{4\exp(-2k_iz_0)}{(k_f+\sqrt{k_f^2+2V})(k_i^2+k_f^2)^2}\ . \tag{65}$$

Therefore, $v(\varepsilon_i,\omega)$ reaches its maximum value, $(8/V)^{1/2}\exp(-2k_iz_0)/k_i^4$, when the initial state is at E_F and when the final state is located at the vacuum level ($\mathbf{k}_f=0$).

For $\varepsilon\le E_F$, the peak in $v(\varepsilon,\omega,k_\parallel)$ should shift to $\omega\approx\Phi+(E_F-\varepsilon)$. However, its absolute value decreases rapidly with decreasing ε, since the amplitude of the wave function which spills out into the outer region of the adlayer-vacuum interface becomes rapidly smaller. Therefore, $\mathrm{Im}d_\perp(\omega)$ shows only a rather broad peak near Φ after the summation over all initial states. For smaller values of z_0, $v(E_F,\omega,k_\parallel)$ in Fig. 9(b) exhibits a strong shoulder on the low-energy side of the peak. As is in Fig. 9(c), this feature is absent in the correspond matrix elements at higher Θ, and thus can be attributed to the intra-atomic transitions to the $3s$-$3p_z$ resonance. However, after the integration over ε, this structure is smeared out, and it is outweighed by the peak at $\omega\approx\Phi$.

The threshold excitation seen in $\mathrm{Im}d_\perp(\omega)$ is therefore a consequence of two factors: (i) the effective potential causing the electronic surface excitations is screened out on the substrate side of the adlayer nuclei, and (ii) the general form of the wave functions near the adlayer-vacuum interface favors transitions for $\omega\approx\Phi$. Because of the importance of the self-consistent surface screening for this threshold feature, it should also be regarded as collective in nature and not as a single-particle phenomenon. We point out here that, because of the large width of the loss function at low coverages, the rapid frequency dependence of the kinematic factor might lead to an effective skewing of the loss profile. Thus, the measured loss features might be shifted from the work function.

It is interesting that the threshold enhancement at low coverages appears as a maximum in $\mathrm{Im}d_\perp(\omega)$ for the alkali adlayers while, in the case of clean Al, it only gives rise to a steplike feature.[31,32] The reason for this difference is presumably the smaller energy range of initial states available within the adsorbate region which contribute to the matrix elements mainly at low frequencies.

In Fig. 10, we show $\mathrm{Im}d_\perp(\omega)$ for hexagonal K adlayers for three coverages. Again, the excitation peak at low Θ is related to Φ, whereas the strong peak at the monolayer coverage at $\omega\sim 3$ eV is due to collective modes. As compared with the spectra for Na, the adsorbate excitation

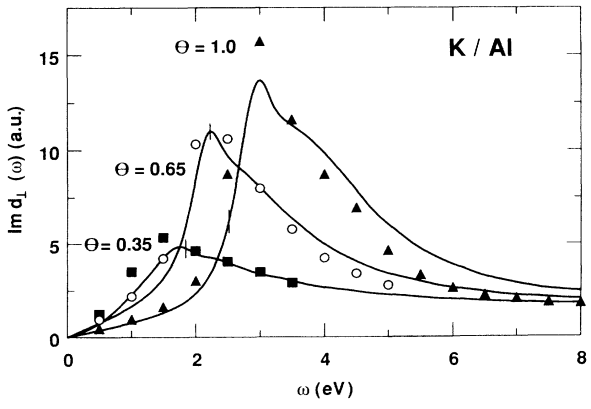

FIG. 10. Imaginary parts of spectral function, $d_\perp(\omega)$, for K-covered jellium surfaces (symbols). The solid lines show $d_\perp(\omega)$ for the corresponding one-dimensional model calculations. The vertical dashes denote the work function.

peaks for K shift to lower energies and become sharper. The latter effect reflects the fact that the adsorbate excitations in K layers couple to electron-hole pairs less strongly than in Na layers because of the larger adlayer-jellium separation. Also, the agreement with the corresponding jellium adlayers becomes somewhat worse than for Na layers: The two-step jellium model overestimates the width of the excitation peaks, and their weight is shifted to higher energies. We suggest that the low-lying d states slightly above E_F which are absent in the jellium model are responsible for this large discrepancy. Nevertheless, apart from these differences, the localized d states do not introduce any characteristic features in $d_\perp(\omega)$. There appears no additional interband or intra-atomic excitation involving K $3d$ states, even at low Θ.

Finally, we turn to the discussion of the second response function $d_\parallel(\omega)$. As stated in Sec. II, for the two-step jellium model, the second term on the right-hand side of (53) vanishes, and the first term gives,[63]

$$d_\parallel(\omega)=z_j+\frac{\bar{n}_a}{\bar{n}}d_a \ . \tag{66}$$

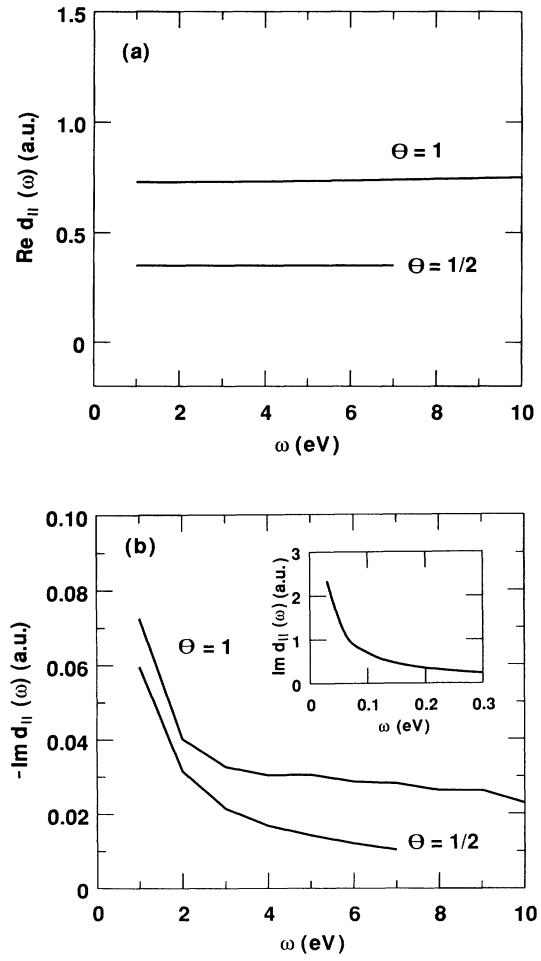

FIG. 11. (a) Real and (b) imaginary parts of spectral function, $d_\parallel(\omega)$, for Na-covered jellium surfaces. The inset shows $\mathrm{Im}d_\parallel(\omega)$ at $\Theta_{\mathrm{Na}}=1$ at very low frequencies.

Equation (66) is derived from a simple argument on charge neutrality. Figure 11 shows the calculated real and imaginary parts of $d_\parallel(\omega)$ for three-dimensional Na adlayers at higher Θ. The deviation of $\mathrm{Re}d_\parallel(\omega)$ from Eq.(66) is seen to be negligibly small in the whole ω range investigated here. Also, the absolute value of $\mathrm{Im}d_\parallel(\omega)$ is two to three orders of magnitude smaller than $\mathrm{Im}d_\perp(\omega)$. Therefore, one can ignore the contribution of $d_\parallel(\omega)$ in the loss function $g(\mathbf{q}_\parallel,\omega)$ in the energy range characteristic of the alkali-metal adsorbate excitations. In the inset of Fig. 11, we show $\mathrm{Im}d_\parallel(\omega)$ at $\Theta_{\mathrm{Na}}=1$ at very low frequencies. This function diverges as $1/\omega$ in the low ω limit. If we write $\mathrm{Im}d_\perp(\omega)$ and $\mathrm{Im}d_\parallel(\omega)$ in the low-frequency limit as

$$\mathrm{Im}d_\perp(\omega)=\xi\frac{\omega}{\omega_p(\mathrm{sub})}, \quad \mathrm{Im}d_\parallel(\omega)=-\eta\frac{\omega_p(\mathrm{sub})}{\omega} \ , \tag{67}$$

we have

$$\mathrm{Im}g(\mathbf{q}_\parallel\omega)=2|\mathbf{q}_\parallel|(\xi+\eta)\frac{\omega}{\omega_p(\mathrm{sub})} \ . \tag{68}$$

We obtained $10^3\eta=6.2$, 3.3, and 4.2 a.u. for $\Theta_{\mathrm{Na}}=\frac{1}{4}$, $\frac{1}{2}$, and 1, respectively. They are negligibly small compared to ξ. Therefore, the low-frequency behavior of $\mathrm{Im}d_\parallel(\omega)$ may be best detected by the resistivity measurement as discussed in Sec. II. For the present system, $l_f\rho=4\pi\eta/\omega_p(\mathrm{sub})=20.5\eta$ a.u. Since $\mathrm{Im}d_\parallel(\omega)$ arises from the inelastic scattering of conduction electrons by adatoms, it is proportional to Θ at very low Θ where multiple-scattering effects can be ignored. It would be enhanced appreciably if the adlayer has a disordered structure instead of the ordered layers assumed in the present study.

IV. SUMMARY

We have studied the dynamical linear-response properties of alkali-metal adlayers on metal surfaces in the long-wavelength limit based on a first-principles method. Realistic three-dimensional Na and K layers in a wide range of coverage values were used as adlayers, and the metal substrate was modeled by semi-infinite jellium with $r_s=2$ corresponding to the electron density of Al. We calculated the density response to a uniform electric field oriented normal to the surface and also the current response to a uniform field parallel to the surface within the time-dependent density-functional theory in order to elucidate how the nature of the adsorbate excitations changes with coverage.

At low Θ, the screening process is dominated by the intra-atomic excitations between adsorbate resonances, and the induced density is strongly localized near the adatoms. However, it was found that these atomiclike transitions are rather broad because of the strong adsorbate-substrate orbital interaction. Thus, in contrast to the traditional picture, these transitions do not lead to any observable features in the electron-energy-loss function. Instead, as a consequence of the surface screening process and matrix-element effects, the loss function at Θ near the work-function minimum exhibits a threshold

enhancement which correlates with the Θ dependence of the work function. Toward monolayer coverage, a strong peak appears in the loss function due to collective excitations localized in the quasi-two-dimensional adlayer because of the formation of wide free-electron-like resonant bands. At monolayer and double-layer coverages, the adlayer-induced collective modes (multipole surface plasmon and adsorbate volume plasmon) are virtually unaffected by the lattice structure of Na and K layers and they are well described within the two-step jellium model.

The plasmon excitations in adsorbed alkali-metal layer have been observed not only on Al as investigated here but also on transition metals and even on semiconductors. In the latter case, the free-electron-like resonant bands of alkali-metal adlayers are strongly modified by the interaction with localized substrate states. Nevertheless, the observed features of the adsorbate response properties in such systems are quite similar to those on Al. It would be interesting to study how the results obtained in the present study using a jellium substrate (delocalized limit) may be generalized to systems involving more localized states.

ACKNOWLEDGMENTS

One of the authors (H.I.) would like to thank the Alexander von Humboldt foundation whose support made this collaboration possible. We are indebted to Dr. S. Blügel for allowing us to use his convergence method. We thank Dr. B. N. J. Persson for valuable discussions on the resistivity problem.

*Permanent address: Institute for Solid State Physics, University of Tokyo, Roppongi, Minato-ku, Tokyo 106, Japan.

[1]P. J. Feibelman, Prog. Surf. Sci. **12**, 287 (1982).
[2]*Electromagnetic Surface Excitations,* edited by R. F. Wallis and G. I. Stegeman (Springer, New York, 1986).
[3]A. U. MacRae, K. Müller, J. J. Lander, J. Morrison, and J. C. Phillips, Phys. Rev. Lett. **22**, 1048 (1969).
[4]S. Andersson and U. Jostell, Faraday Discuss. Chem. Soc. **60**, 255 (1975).
[5]S. A. Lindgren and L. Walldén, Phys. Rev. B **4**, 5967 (1980).
[6]J. Cousty, R. Riwan, and P. Soukiassian, J. Phys. (Paris) **46**, 1693 (1985).
[7]T. Aruga, H. Tochihara, and Y. Murata, Phys. Rev. B **34**, 8237 (1986).
[8]A. Hohlfeld, M. Sunjic, and K. Horn, J. Vac. Sci. Technol. A **5**, 679 (1987).
[9]D. Heskett, K. H. Frank, K. Horn, E. E. Koch, H. J. Freund, A. Baddorf, K. D. Tsuei, and E. W. Plummer, Phys. Rev. B **37**, 10 387 (1989).
[10]D. L. Seymour, C. F. McConville, D. P. Woodruff, and J. E. Inglesfield, Surf. Sci. **214**, 57 (1989).
[11]J. W. Gadzuk, Phys. Rev. B **1**, 1267 (1970).
[12]D. M. Newns, Phys. Lett. **39A**, 341 (1972).
[13]J. E. Inglesfield and E. Wikborg, J. Phys. F **5**, 1706 (1975).
[14]M. Nakayama, T. Kato, and K. Ohtomi, Solid State Commun. **50**, 409 (1984).
[15]A. G. Eguiluz and A. Campbell, Phys. Rev. B **31**, 7572 (1985).
[16]H. Ishida and M. Tsukada, Surf. Sci. **169**, 225 (1986).
[17]K. Kempa and W. L. Schaich, Solid State Commun. **61**, 357 (1987).
[18]R. Fuchs and W. Ekardt, J. Phys. Condens. Matter **1**, 4081 (1989).
[19]B. N. J. Persson and L. H. Dubois, Phys. Rev. B **39**, 8220 (1989).
[20]A. Liebsch, Phys. Rev. B **40**, 3421 (1989).
[21]A. Liebsch, G. Hincelin, and T. López-Ríos, Phys. Rev. B **41**, 10 463 (1990).
[22]A. Liebsch, Phys. Rev. Lett. **67**, 2858 (1991).
[23]J. A. Gaspar, A. G. Eguiluz, K. D. Tsuei, and E. W. Plummer, Phys. Rev. Lett. **67**, 2854 (1991); A. G. Eguiluz and J. A. Gaspas, in *Lectures in Surface Physics,* edited by M. Cardona and F. Ponce (Springer, Heidelberg, in press).
[24]H. P. Bonzel, Surf. Sci. Rep. **8**, 43 (1987).
[25]*Alkali Adsorption on Metals and Semiconductors,* edited by H. P. Bonzel, A. M. Bradshaw, and G. Ertl (Elsevier, Amsterdam, 1989).
[26]T. Aruga and Y. Murata, Prog. Surf. Sci. **31**, 61 (1989).
[27]P. J. Feibelman, Phys. Rev. B **14**, 762 (1976); **23**, 2629 (1981).
[28]P. Apell, Phys. Scr. **24**, 795 (1981).
[29]W. L. Schaich and W. Chen, Phys. Rev. B **39**, 10 714 (1989).
[30]N. D. Lang, in *Theory of the Inhomogeneous Electron Gas,* edited by S. Lundqvist and N. H. March (Plenum, New York, 1983).
[31]A. Liebsch, Phys. Rev. B **36**, 7378 (1987); J. Phys. C **19**, 5025 (1986).
[32]K. Kempa and W. L. Schaich, Phys. Rev. B **37**, 6711 (1988); **39**, 13 139 (1989).
[33]A. Liebsch, Phys. Rev. B **32**, 6255 (1985).
[34]B. N. J. Persson and A. Apell, Phys. Rev. B **27**, 6058 (1983).
[35]B. N. J. Persson and E. Zaremba, Phys. Rev. B **30**, 5669 (1984).
[36]E. Levinson, E. W. Plummer, and P. J. Feibelman, Phys. Rev. Lett. **43**, 952 (1979).
[37]K. D. Tsuei, E. W. Plummer, A. Liebsch, K. Kempa, and P. Bakshi, Phys. Rev. Lett. **64**, 44 (1990); K. D. Tsuei, E. W. Plummer, A. Liebsch, E. Pehlke, K. Kempa, and P. Bakshi, Surf. Sci. **247**, 302 (1991).
[38]R. Del Sole and E. Fiorino, Phys. Rev. B **29**, 4631 (1984).
[39]W. L. Mochan and R. Barrera, Phys. Rev. B **32**, 4984 (1985); **32**, 4989 (1985).
[40]R. E. Palmer, J. F. Arnett, and R. Willis, Phys. Rev. Lett. **58**, 2490 (1987).
[41]A. Muramatsu and W. Hanke, in *Structure and Dynamics of Surfaces II,* edited by W. Schommers and P. von Blanckenhagen, Topics in Current Physics Vol. 43 (Springer, New York, 1987).
[42]J. T. Lee and W. L. Schaich, Phys. Rev. B **43**, 4629 (1991).
[43]N. D. Lang, Phys. Rev. B **4**, 4234 (1971).
[44]H. Ishida and A. Liebsch, Phys. Rev. B **42**, 5505 (1990).
[45]W. Kohn and L. J. Sham, Phys. Rev. **140**, A1133 (1965); P. Hohenberg and W. Kohn, *ibid.* **136**, B864 (1964).
[46]H. Ishida, Phys. Rev. B **42**, 10 899 (1991).
[47]A. Zangwill and P. Soven, Phys. Rev. A **21**, 1561 (1980); M. J. Stott and E. Zaremba, *ibid.* **21**, 12 (1980); G. D. Mahan, *ibid.* **22**, 1780 (1980).
[48]N. D. Lang and A. R. Williams, Phys. Rev. B **18**, 616 (1978); **16**, 2408 (1977).
[49]B. N. J. Persson, Phys. Rev. B **44**, 3277 (1991); B. N. J.

Persson, D. Schumacher, and A. Otto, Chem. Phys. Lett. **178**, 204 (1991).

[50]*Thin Metal Films and Gas Chemisorption,* edited by P. Wissman (Elsevier, Amsterdam, 1987).

[51]H. Ishida and A. Liebsch (unpublished).

[52]H. Hjelmberg, O. Gunnarsson, and B. I. Lundqvist, Surf. Sci. **68**, 158 (1977); O. Gunnarsson, H. Hjelmberg, and J. K. Nørskov, Phys. Scr. **22**, 165 (1980).

[53]J. E. Inglesfield, J. Phys. C **14**, 3795 (1981); J. E. Inglesfield and G. A. Benesh, Phys. Rev. B **37**, 6682 (1988).

[54]G. B. Bachelet, D. R. Hamann, and M. Schlüter, Phys. Rev. B **26**, 4199 (1982).

[55]J. E. Inglesfield, Surf. Sci. **76**, 355 (1978).

[56]We use Wigner's interpolation formula for the local exchange-correlation potential functional.

[57]R. S. Sorbello, Solid State Commun. **56**, 821 (1985); **48**, 989 (1983).

[58]S. Blügel (unpublished).

[59]A. A. Lucas and M. Sunjic, Phys. Rev. Lett. **26**, 229 (1971).

[60]H. Ishida, Phys. Rev. B **38**, 8006 (1989).

[61]G. M. Lamble, R. S. Brooks, D. A. King, and D. Norman, Phys. Rev. Lett. **61**, 1112 (1988).

[62]B. N. J. Persson and E. Zaremba, Phys. Rev. B **31**, 1863 (1985).

[63]P. Apell, A. Lyungbert, and S. Lundqvist, Phys. Scr. **30**, 367 (1984).